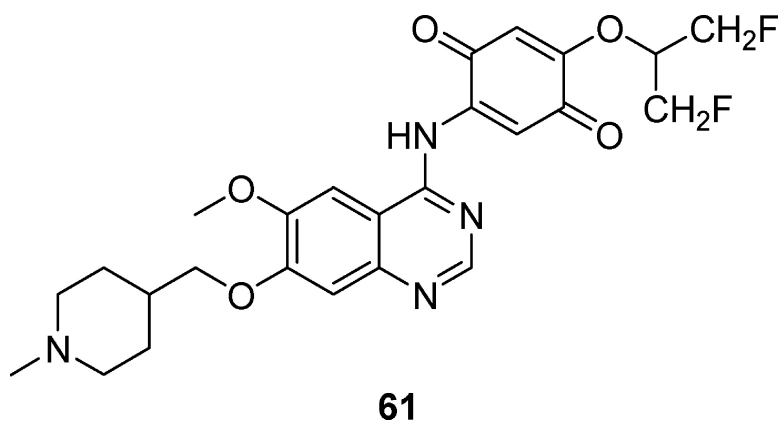


2-(Quinazolin-4-ylamino)-[1,4]benzoquinones as Covalent-Binding, Irreversible Inhibitors of the Kinase Domain of Vascular Endothelial Growth Factor Receptor-2

Allan Wissner, M. Brawner Floyd, Bernard D. Johnson, Heidi Fraser, Charles Ingalls, Thomas Nittoli, Russell G. Dushin, Carolyn Discafani, Ramaswamy Nilakantan, Joseph Marini, Malini Ravi, Kinwang Cheung, Xingzhi Tan, Sylvia Musto, Tami Annable, Marshall M. Siegel, and Frank Loganzo

J. Med. Chem., **2005**, 48 (24), 7560-7581 • DOI: 10.1021/jm050559f • Publication Date (Web): 03 November 2005

Downloaded from <http://pubs.acs.org> on March 29, 2009



More About This Article

Additional resources and features associated with this article are available within the HTML version:

- Supporting Information
- Links to the 2 articles that cite this article, as of the time of this article download
- Access to high resolution figures
- Links to articles and content related to this article
- Copyright permission to reproduce figures and/or text from this article

[View the Full Text HTML](#)

2-(Quinazolin-4-ylamino)-[1,4]benzoquinones as Covalent-Binding, Irreversible Inhibitors of the Kinase Domain of Vascular Endothelial Growth Factor Receptor-2

Allan Wissner,* M. Brawner Floyd, Bernard D. Johnson, Heidi Fraser, Charles Ingalls, Thomas Nittoli, Russell G. Dushin, Carolyn Discafani, Ramaswamy Nilakantan, Joseph Marini, Malini Ravi, Kinwang Cheung, Kingzhi Tan, Sylvia Musto, Tami Annable, Marshall M. Siegel, and Frank Loganzo

Chemical and Screening Sciences and Oncology Research, Wyeth Research, 401 N. Middletown Road, Pearl River, New York 10965

Received June 13, 2005

A series of 2-(quinazolin-4-ylamino)-[1,4] benzoquinone derivatives that function as potent covalent-binding, irreversible inhibitors of the kinase domain of vascular endothelial growth factor receptor-2 (VEGFR-2) has been prepared by ceric ammonium nitrate oxidation of substituted (2,5-dimethoxyphenyl)(6,7-disubstituted-quinazolin-4-yl)amines and by displacement of the chlorine atom of substituted 2-chloro-5-(6,7-disubstituted-quinazolin-4-ylamino)-[1,4]benzoquinones with various amines, anilines, phenols, and alcohols. Enzyme studies were conducted in the absence and presence of glutathione and plasma. Several of the compounds inhibit VEGF-stimulated autophosphorylation in intact cells. Kinetic experiments were performed to study the reactivity of selected inhibitors toward glutathione. Reactivities correlated with LUMO energies calculated as averages of those of individual conformers weighted by the Boltzmann distribution. These results and molecular modeling were used to rationalize the biological observations. The compounds behave as non-ATP-competitive inhibitors. Unequivocal evidence, from mass spectral studies, indicates that these inhibitors form a covalent interaction with Cys-1045. One member of this series displays antitumor activity in an *in vivo* model.

Angiogenesis is the process of new blood vessel growth. Several biological effectors mediate angiogenesis, including various growth factors and their receptors.¹ Vascular endothelial growth factor receptor-2 (VEGFR2), also known as KDR, is a receptor tyrosine kinase expressed on the endothelial cells that comprise blood vessels.² Solid tumors require vascularization in order to grow beyond a small size and to metastasize; therefore, many tumors express and secrete growth factors, including VEGF, to promote blood vessel development.^{3,4} Animal studies support a critical role for the paracrine activation of VEGFR-2 by its ligand, VEGF, in tumor neovascularization, growth, and metastasis. In patient tumor samples, VEGF or VEGFR-2 has been shown to be elevated and negatively correlates with survival.⁵

The proposed clinical benefit of therapeutics that inhibit angiogenesis has been widely reviewed. For example, such therapy may produce less drug resistance by targeting untransformed endothelial cells rather than genetically unstable cancer cells and also may be effective when drug resistance has already developed.^{6,7} In addition, slowly growing tumors are often refractory to standard cytotoxic cancer therapy but responsive to continuous, low-dose antiangiogenic drugs.⁸ Furthermore, by primarily targeting the vasculature rather than the tumor, expression of the target by the tumor itself is not required.

In animal models, inhibition of VEGFR-2 and/or VEGF effectively inhibits the growth of solid tumors derived from lung, colorectal, breast, prostate, and other tissues. Neutralizing antibodies to VEGF (e.g., bevacizumab) or to VEGFR-2 (e.g., DC101) inhibit primary tumor growth and/or the incidence of metastases *in vivo*.^{9,10} Combinations with standard cytotoxic drugs, such as paclitaxel, can improve efficacy. Ribozymes or RNA interference (RNAi) constructs that specifically decrease VEGF or VEGFR-2 levels have demonstrated activity in cellular, angiogenesis, or animal models.^{11–13}

Effort has also focused on the design and development of small molecule inhibitors of VEGFR-2 kinase, several of which are in clinical development.^{14,15} Lead molecules inhibit purified recombinant VEGFR-2 kinase with $IC_{50} < 100$ nM. Many of these small molecule inhibitors are also nonselective against related kinases, which may be of benefit, since some of these kinases have been implicated in tumor growth and angiogenesis. The reported VEGFR-2 kinase inhibitors decrease VEGFR-2 phosphorylation in cells and/or inhibit VEGF-stimulated growth of cultured endothelial cells. Activity is frequently demonstrated in alternative angiogenesis models. VEGFR-2 kinase inhibitors also slow the growth of human tumor xenografts in rodents.

Phase I clinical trials of single-agent antibody or small molecule inhibitors of VEGFR-2 or VEGF have shown these agents to be generally well tolerated. In phase II/III trials in patients with solid tumors, stable disease and partial regressions have been observed with small

* Corresponding author. Tel: (845) 602-3580. Fax: (845) 602-5561. E-mail: wissnea@wyeth.com.

molecule VEGFR-2 inhibitors, either as monotherapy or in combinations.^{16–18} In combination with chemotherapeutics, the anti-VEGF antibody bevacizumab produced complete regressions and increased survival time in colorectal cancer patients¹⁹ and increased response rate in some lung cancers.²⁰ These data in patients help to validate inhibition of the VEGF pathway as a potentially useful method to control some forms of cancer.

In earlier studies, using molecular modeling, we had some success in developing covalent binding inhibitors of two growth factor receptor kinases, EGFR and HER-2. Two of these structurally related inhibitors are currently in clinical trial.^{21–24} These inhibitors function as irreversible binding inhibitors by virtue of the fact that they form a covalent interaction with a conserved Cys residue (Cys-773 in EGFR and Cys-805 in HER-2) located near the ATP binding pocket of these enzymes. With the availability of the X-ray crystal structure of the catalytic domain of VEGFR-2,²⁵ we thought that it might be possible to design covalent binding inhibitors of this enzyme, provided that there was present, at the ATP binding site, a Cys residue that would be accessible to a bound inhibitor.

It has been reported that the quinazoline-based kinase inhibitors are effective inhibitors of VEGFR-2.²⁶ Additionally, there is extensive knowledge, derived from molecular modeling studies and experimental data, that shows how this class of inhibitors binds at the active site of kinases.^{27–29} We therefore decided to use the quinazoline core structure as the foundation for the construction of these covalently binding VEGFR-2 inhibitors. Accordingly, we docked the known VEGFR-2 inhibitor **1** (ZD-4190), reported by the Zeneca group,³⁰ into the active site of VEGFR-2, as shown in Figure 1. The molecule was oriented at the site in a manner consistent with what is known about how these types of inhibitors bind to kinases. While it was immediately obvious that the Cys residue that we targeted in EGFR and HER-2 was not conserved in VEGFR-2, we did note that there appears to be an accessible Cys residue, Cys-1045, located near the 4-anilino group of the inhibitor. This suggested that it might be possible to design a quinazoline-based inhibitor that could function as a covalent-binding inhibitor of VEGFR-2, by replacing the 4-anilino substituent with an appropriately reactive group approximately the same size as the anilino substituent. We also noted that there are certain other kinases of interest that are also involved in angiogenesis, such as PDGFR and VEGFR1, where a Cys residue homologous to Cys-1045 is conserved. The inhibitors we describe herein potentially could also function as covalent binding inhibitors of these targets.

We prepared a number of quinazoline derivatives where we surveyed different types of reactive groups attached at the 4-position of the quinazoline core. Among the most biologically active compounds were a series, based on structure **2**, where the phenyl ring of the 4-anilino substituent of a conventional quinazoline inhibitor had been replaced with a quinone ring, resulting in a series of 2-(quinazolin-4-ylamino)-[1,4]benzoquinones.

We realized from the onset that a quinone moiety can be a highly reactive type of substituent and that the

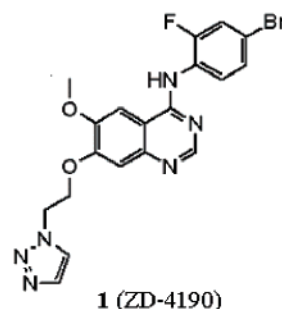
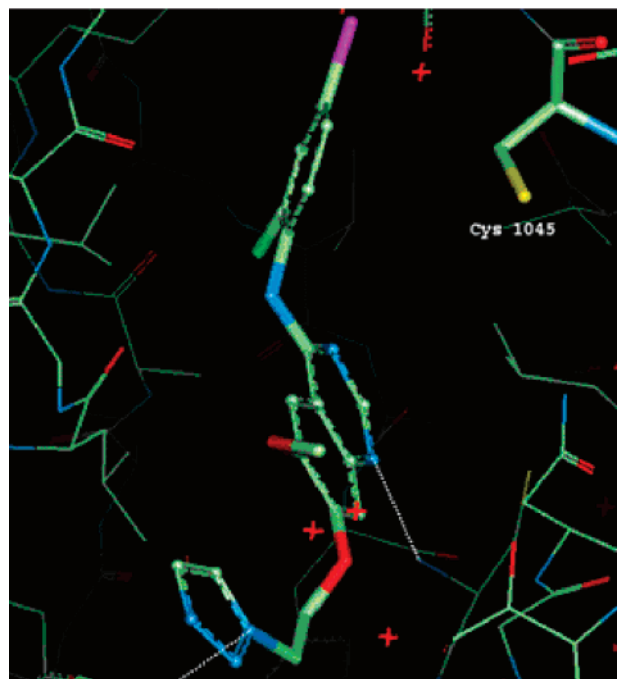


Figure 1. Binding model of **1**³⁰ at the active site of VEGFR-2. Note the proximity of Cys-1045 to the 4-anilino substituent.

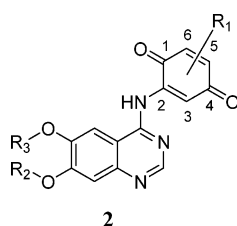
potentially high reactivity of these quinone-based inhibitors would be a major issue in designing an entity with druglike properties. Nevertheless, we felt that we might be able to moderate the reactivity of this type of inhibitor, to the required degree, by choosing appropriate substituents on the quinone ring. One assumption inherent in any such approach involving the use of a highly electrophilic species as a potential drug is that the drug needs to be more reactive toward the target enzyme than it is toward other nucleophilic species [such as glutathione (GSH)] that may be present in high concentrations in the circulation or in the cytosol. Assuming that these quinone-based inhibitors bind as proposed with the quinone ring located nearby Cys-1045, we can rely on an anticipated entropic effect wherein the reactivity of such an inhibitor, when bound at the active site, will be enhanced relative to its reactivity in solution due to the two reactive centers being held in close proximity. In addition, one could speculate that a drug based on a moderately reactive irreversible inhibitor might not need to exhibit a half-life in circulation comparable to that of a conventional inhibitor, since once the target is deactivated by the covalent interaction, the drug need not be present in circulation to sustain the desired inhibitory activity. In

effect, the duration of action of such a drug will be a function of the rate of receptor turnover.

In this paper, we will describe our work on this class of compounds. We will discuss the syntheses of members of this series, describe the results of reactivity studies, and show how they relate to the biological properties of these inhibitors. The results of molecular orbital calculations and molecular modeling were used to rationalize the experimental observations. Additionally, we will present our evidence suggesting that these inhibitors do indeed bind in a covalent manner. Finally, we will show that one member of this series displays antitumor activity in an *in vivo* model.

Chemistry

The numbering of the carbon atoms of the quinone ring used in the discussion that follows is as indicated in structure **2**. While this numbering system may not



always conform to the proper numbering, keeping the ring numbers constant at the same positions between compounds will help clarify the discussion. The proper ring numbering was used in naming the compounds in the Experimental Section.

In our preliminary work, we confined our efforts to optimize the quinone substituents with respect to the reactivity and *in vitro* biological activity of the inhibitors. We therefore decided to keep the substituents at the 6 and 7 positions of the quinazoline constant during this optimization phase. In this initial effort, we made quinazolines with 6-methoxy-7-(2-methoxyethoxy) substituents. Later, only after we had a better understanding of the SAR of the quinone moiety, did we alter the side chain at the 6 and 7 positions of the quinazoline ring in an attempt to improve the bioavailability of the molecules. Additionally, since we knew that the high reactivity of these inhibitors would be an issue with respect to them functioning in cellular or *in vivo* assays, we concentrated our efforts toward the synthesis of less reactive quinone derivatives, that is, quinones with electron-donating substituents. As will be discussed in detail later, electron-donating substituents on the quinone ring usually will raise the LUMO energy of these molecules and thereby decrease their reactivity.

The key formamidine intermediate **6** (Scheme 1) was simply prepared by alkylation of 4-hydroxy-3-methoxybenzotrile with 1-bromo-2-methoxyethane using NaH in DMF. The resulting compound **3** could be nitrated selectively, giving **4**, which after catalytic reduction furnished the aniline derivative **5**. Condensation of **5** with dimethylformamide–dimethylacetal (DMF–DMA) furnished **6**. Cyclization to the quinazoline and incorporation of the 4-anilino group was accomplished in a single step by refluxing **6** with the substituted anilines **7a,b,e–h,k–m** in acetic acid to give the respective products **8a,b,e–h,k–m**. These intermediates, in turn,

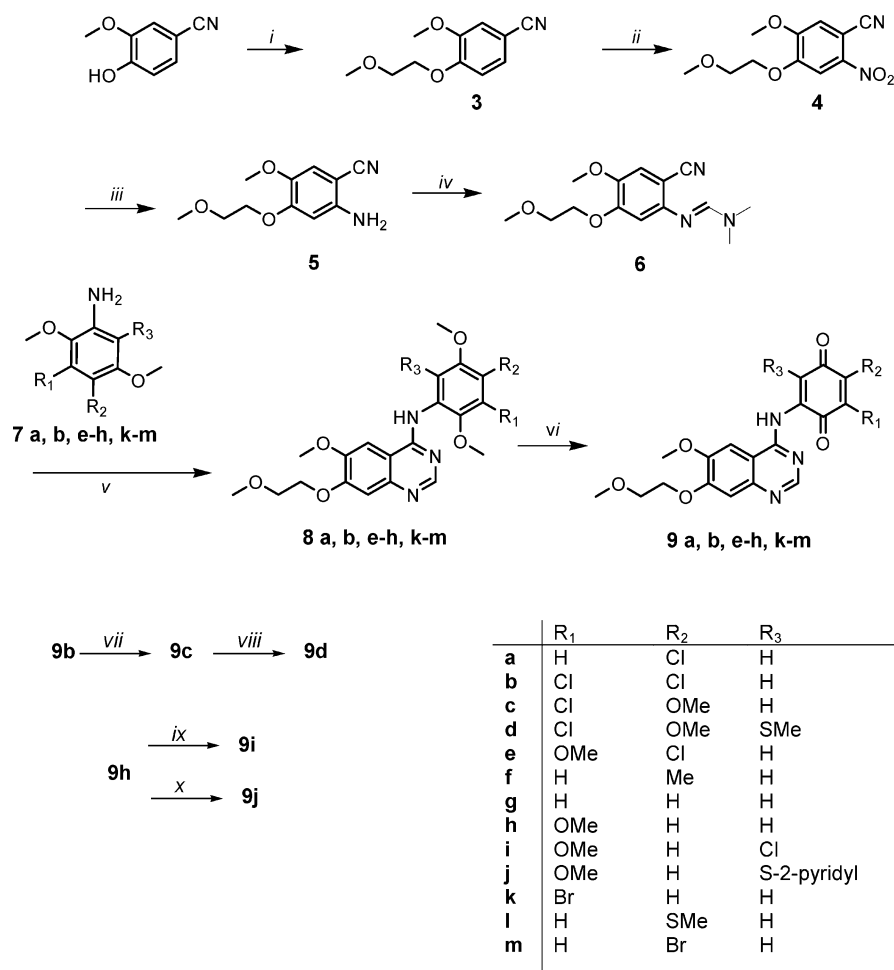
were then oxidized with ceric ammonium nitrate (CAN) in aqueous CH₃CN to give the respective quinone derivatives **9a,b,e–h,k–m**.

Some of the quinone inhibitors thus prepared also served as intermediates to prepare other members of the series. For example, **9b** can be converted to **9c** by the reaction with sodium phenoxide in methanol. Additionally, treatment of **9c** with methylmercaptan in CH₂Cl₂ resulted in an initial reductive addition product that was reoxidized *in situ* with DDQ to furnish the 6-chloro-5-methoxy-3-thiomethyl derivative **9d**. In a similar manner, involving an initial reductive addition followed by a reoxidation, inhibitors **9i** and **9j** were obtained. For reactions involving **9h** with nucleophiles, the reductive additions occurred at the 3-position of the quinone ring. For the derivative **9j**, the regiochemistry was confirmed by a NOESY NMR experiment, where we observed an interaction between the methoxy group and the hydrogen atom at the 5-position. The regiochemistry of the product **9i** resulting from hydrogen chloride addition to **9h** followed by reoxidation was confirmed by a NOESY experiment and, later, by an independent synthesis of the other regioisomer **9c**.

The quinone derivatives **9a** and **9b**, having a chlorine atom at the 5-position, proved to be very versatile intermediates, since the chlorine atom could be displaced with a variety of nucleophiles, resulting in the inhibitors shown in Scheme 2. Depending on the type of nucleophile, different methods were used to effect these displacements. The phenoxy-substituted derivative **13** was prepared by treating **9a** with phenol and K₂CO₃ in acetone at room temperature (method D). The other phenoxy-substituted inhibitors, **18–20**, were prepared using phase-transfer conditions, where the phenol and **9a** were stirred in a two-phase mixture of 1 N NaOH and CH₂Cl₂ in the presence of the phase-transfer catalyst Aliquat-336 (tricaprylylmethylammonium chloride) at room temperature (method F).

The inhibitor **12** was prepared simply by stirring a solution of **9a** and an excess of the *N*-methylaniline in THF or glyme (method B). Inhibitors containing a dialkylamino group at the 5-position of the quinone were prepared by one of two methods. Simply stirring a solution of **9a** and an excess of the dialkylamine in THF or dioxane using pyridine hydrochloride as a catalyst produced the inhibitors **10** and **21–25** (method A). The exact conditions used with respect to time and temperatures are discussed in detail in the Experimental Section. The other 5-amino substituted derivatives, such as **11** and **17**, were prepared from **9a** in a similar manner without using a catalyst (method B).

The remaining compounds shown in Scheme 2 are those having a 5-alkoxy group attached to the quinone ring. These inhibitors, **26–40**, were prepared by stirring a CH₂Cl₂ solution of **9a,b** with an excess of the alcohol in the presence of at least 1 equiv of sodium phenoxide–(H₂O)₃ (method E). By observing the mass spectrum at different time intervals, we monitored the course of several of these reactions. We observed the initial formation of the phenoxy derivative **13** followed by a subsequent buildup of the 5-alkoxy-substituted product and an associated decrease in **13**. Thus, under these conditions, the substitution reaction proceeds through the intermediacy of **13**. Indeed, treatment of **13** directly

Scheme 1^a

^a (i) NaH, CH₃OCH₂CH₂Br, DMF, 70 °C, 5.5 h. (ii) TFAA/CHCl₃, NH₄NO₂, reflux, 2 h. (iii) Cyclohexene, Pd/C, EtOH, reflux, 24 h. (iv) DMF–DMA, 100 °C, 5 h. (v) AcOH, reflux. (vi) Ce(NH₄)₂(NO₃)₆, H₂O, MeCN, rt. (vii) ROH, NaOPh(3H₂O), CH₂Cl₂, rt. (viii) (1) MeSH, CH₂Cl₂; (2) DDQ, CH₂Cl₂. (ix) (1) HCl, CHCl₃, rt, overnight; (2) DDQ, NaOAc, MeCN, H₂O, 1 h, rt. (x) (1) 2-mercaptopyridine, CHCl₃, 0.5 h; (2) DDQ, MeCN.

with alcohols and a base catalyst resulted in the formation of **14–16**.

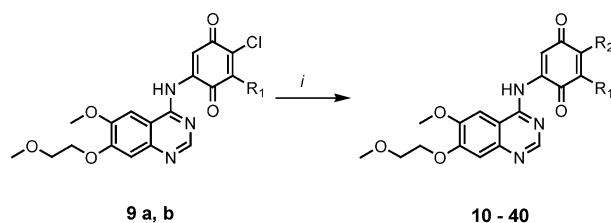
Treatment of the 5-(*N*-aziridinyl)-substituted derivative **21** with hydrochloric acid in THF resulted in hydrolytic ring opening, giving the 2-hydroxypropylamino-substituted inhibitor **41**. This, in turn, was converted to the oxazolidin-2-one derivative **42** by reaction with carbonyl diimidazole.

The substituted aniline **7e** needed to prepare **9e** was itself prepared starting with the known substituted benzaldehyde **43**³¹ (Scheme 3). The acetate group of **43** was converted to a methoxy group by adding a KOH solution to a solution of the compound in EtOH in the presence of dimethyl sulfate, resulting in **44**. This compound was then selectively demethylated with LiCl in hot DMF. The resulting intermediate **45** was then oxidized to the hydroquinone derivative **46** using basic H₂O₂. The free hydroxyl groups were then re-methylated with dimethyl sulfate and K₂CO₃ in DMF and the nitro group was reduced with iron and acetic acid in refluxing MeOH, giving the desired intermediate **7e**. This was used to prepare **9e** as described above.

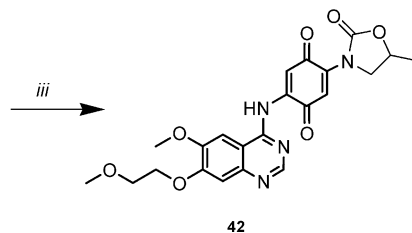
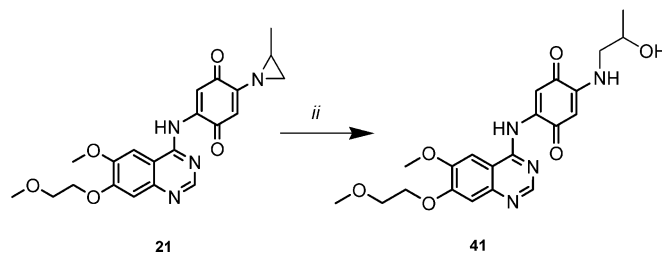
The reaction of **9e** with an excess of some alcohols using cesium carbonate in methylene chloride gave unanticipated results. The reaction with methanol or 1,3-difluoropropan-3-ol gave the expected products, **49**

and **50**, respectively, resulting from displacement of the chlorine atom of **9e**, while the reaction with 2-propanol gave **52**, the result of displacement of the methoxy group of **9e**. The reaction of **9e** with cyclopropylmethanol gave a mixture of displacement products **48** and **51**, although only **51** was obtained in a pure state. The dependence of the regiochemistry of the displacement products on the nature of the alcohol used is curious and, frankly, we cannot offer a good rationale for these results.

Having explored the reactivity issues and the SAR resulting from alterations of the substituents on the quinone ring, we next turned our attention to modifications of the 6- and 7-positions of the quinazoline ring. It is well-known that modifications at these two positions have an important influence on the water solubility and bioavailability of these quinazoline-based kinase inhibitors.^{22,24,26,32} We prepared inhibitors that retain the 6-methoxy group of the quinazoline while having a basic side chain at the 7-position. The preparation of the chloroquinone intermediates **59a,b** needed to prepare these compounds is shown in Scheme 4. We developed a flexible synthesis that allows the 7-substituent to be altered by utilizing the relatively advanced intermediate **56**. Reductive amination utilizing aldehyde **53** and aniline **7a** gave the required intermediate **54**. This was condensed with the known³³ 4-chloro-

Scheme 2^a

	Method ⁱ	R ₁	R ₂		Method ⁱ	R ₁	R ₂	
i	10	A	H	N(Me) ₂	26	E	H	OCH(CH ₂ F) ₂
	11	B	H	<i>N</i> -Morpholinyl	27	E	H	OCH ₂ -3-pyridyl
	12	B	H	N(Me)Ph	28	E	H	O(CH ₂) ₂ OPh
	13	D	H	OPh	29	E	H	OCH(CH ₃) ₂
	14	C	H	O(CH ₂) ₂ OMe	30	E	Cl	OCH(CH ₂ F) ₂
	15	C	H	OCH ₂ Ph	31	E	Cl	OCH ₂ Ph-3-F
	16	C, E	H	OMe	32	E	Cl	OEt
	17	B	H	<i>N</i> -Piperidinyl	33	E	H	OCH ₂ Ph-2-F
	18	F	H	OPh-4- <i>N</i> -imidazolyl	34	E	H	OCH ₂ Ph-3-F
	19	F	H	OPh-3-F	35	E	H	OCH ₂ Ph-4-F
	20	F	H	OPh-3- <i>N</i> -Et	36	E	H	OEt
	21	A	H	<i>N</i> -Aziridinyl-2-methyl	37	E	H	OCH(CF ₃)Ph
	22	A	H	<i>N</i> -Piperidinyl-4-CH ₂ Ph	38	E	H	OCH ₂ C ₆ F ₅
	23	A	H	<i>N</i> -Piperazinyl-4-CH ₂ Ph	39	E	H	OCH ₂ CHF ₂
	24	A	H	<i>N</i> -Piperazinyl-4-Et	40	E	H	OCH ₂ CCPh
25	A	H	<i>N</i> -Pyrrolidinyl					

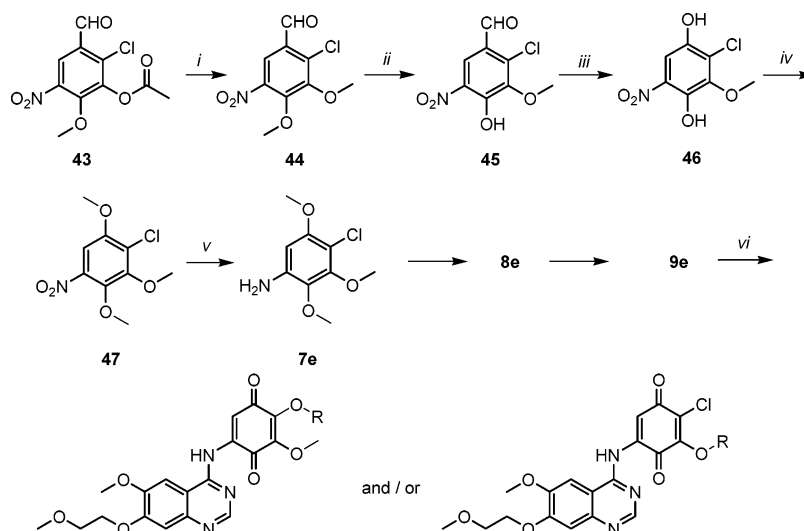


^a (i) Method A: R₂NH or RNH₂, pyridine hydrochloride, THF or dioxane. Method B: R₂NH or RNH₂, THF or ethylene glycol dimethyl ether. Method C: ROH, Et₃N, CH₂Cl₂, 60 °C. Method D: ROH, K₂CO₃, acetone, rt. Method E: ROH, NaOPh(3H₂O), CH₂Cl₂, rt. Method F: ROH, 1 M NaOH, CH₂Cl₂, rt, Aliquat 336. (ii) HCl, THF, H₂O, 18 h, rt. (iii) Carbonyl diimidazole, 1-methyl-2-pyrrolidinone, 80 °C, 27 h.

7-fluoro-6-methoxyquinazoline, **55**, in a mixture of refluxing pyridine-*tert*-butyl alcohol to give **56**. The fluorine atom of **56** could be readily displaced by utilizing sodium alkoxides derived from alcohols **57a,b**. The products of these displacements were not purified but were directly deprotected using TFA to give the intermediates **58a,b**; these in turn, were oxidized with CAN to the quinones **59a,b** as described previously.

Displacement of the 5-chloro substituent in **59a,b** with various alcohols utilizing the methods already discussed gave the inhibitors **60–75** shown in Scheme 5.

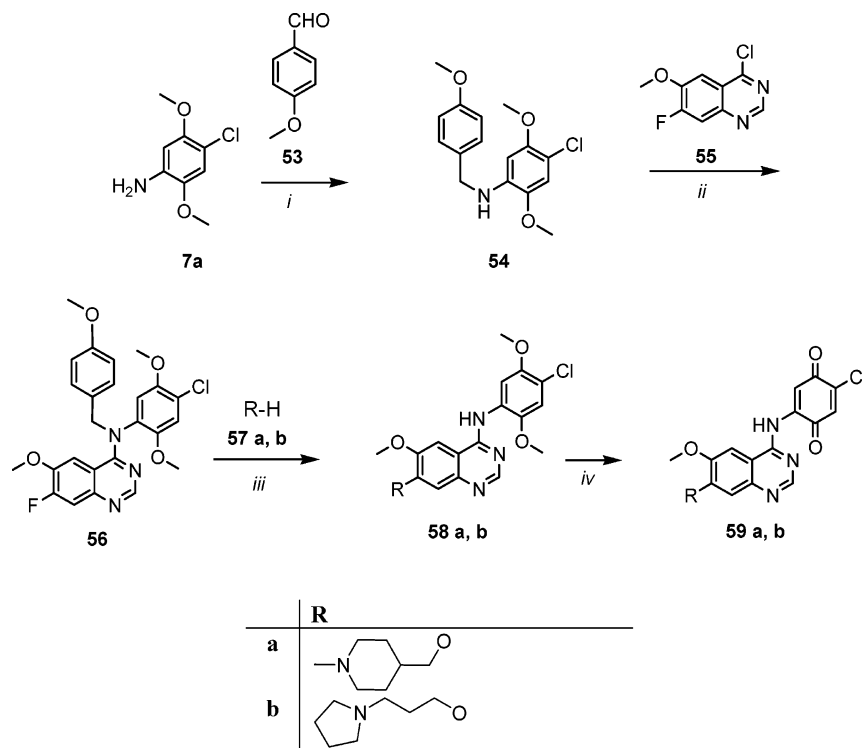
Reactivity Studies. Since we are proposing that these quinone derivatives function as covalent-binding inhibitors, information about the reactivity of these compounds toward sulfur-containing nucleophiles would be of obvious interest. Nucleophiles of major importance

Scheme 3^a

	R
48	CH ₂ -cyclopropyl
49	CH ₃
50	CH(CH ₂ F) ₂

	R
51	CH ₂ -cyclopropyl
52	CH(CH ₃) ₂

^a (i) EtOH, (Me)₂SO₄, 40% KOH, 55 °C, 1 h. (ii) LiCl, DMF, H₂O, 110 °C, 3 h. (iii) 1 N NaOH, H₂O, H₂O₂, MeOH, 50 °C, 3.5 h. (iv) (Me)₂SO₄, K₂CO₃, DMF, 80 °C, 1 h. (v) MeOH, Fe, AcOH, reflux, 2 h. (vi) ROH, CsCO₃, CH₂Cl₂, rt.

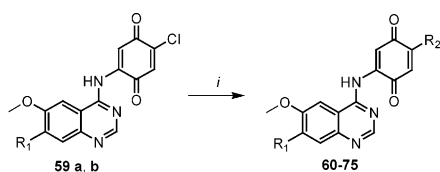
Scheme 4^a

	R
a	
b	

^a (i) AcOH, NaBH(OAc)₃, 1,2-dichloroethane, 2.5 h, rt. (ii) pyridine, *t*-BuOH, 24 h, reflux. (iii) (1) NaHMDS, THF; (2) TFA. (iv) CAN, MeCN, H₂O, rt.

would be Cys-1045 of the target protein and, perhaps, other sulfhydryl-containing species, such as glutathione, which is expected to be present at high concentrations in the circulation or the cytosol. According to frontier molecular orbital theory, a major component of the

reactivity of such a system would be determined by the difference in energy between the HOMO of the nucleophile and the LUMO of the electrophile. The smaller this HOMO–LUMO gap the more reactive the system is expected to be. Since in the discussions to follow,

Scheme 5^a

	Method ⁱ	R ₁	R ₂
60	C	OCH ₂ -4-piperidinyl-1-methyl	OMe
61	C	OCH ₂ -4-piperidinyl-1-methyl	OCH(CH ₂ F) ₂
62	G	OCH ₂ -4-piperidinyl-1-methyl	O(CH ₂) ₂ NMePh
63	G	OCH ₂ -4-piperidinyl-1-methyl	OCH ₂ Ph
64	C, G	O(CH ₂) ₃ - <i>N</i> -pyrrolidinyl	OMe
65	E	O(CH ₂) ₃ - <i>N</i> -pyrrolidinyl	OCH(CH ₂ F) ₂
66	E	O(CH ₂) ₃ - <i>N</i> -pyrrolidinyl	OCH ₂ CCPh
67	E	O(CH ₂) ₃ - <i>N</i> -pyrrolidinyl	OCH ₂ -2-Pyridyl
68	E	O(CH ₂) ₃ - <i>N</i> -pyrrolidinyl	OCH ₂ Ph
69	E	O(CH ₂) ₃ - <i>N</i> -pyrrolidinyl	OCH ₂ C ₆ F ₅
70	E	O(CH ₂) ₃ - <i>N</i> -pyrrolidinyl	OCH(Ph)CCH
71	E	O(CH ₂) ₃ - <i>N</i> -pyrrolidinyl	OCH ₂ CCH
72	E	O(CH ₂) ₃ - <i>N</i> -pyrrolidinyl	OCH ₂ CHCH ₂
73	E	O(CH ₂) ₃ - <i>N</i> -pyrrolidinyl	OCH(Me)CCH
74	E	O(CH ₂) ₃ - <i>N</i> -pyrrolidinyl	OCH ₂ -2-furyl
75	E	O(CH ₂) ₃ - <i>N</i> -pyrrolidinyl	OCH ₂ CHF ₂

^a (i) Method C: ROH, Et₃N, CH₂Cl₂, 60 °C. Method E: ROH, NaOPh(3H₂O), CH₂Cl₂, rt. Method G: ROH, CsCO₃, CHCl₃, rt.

where the nucleophile is kept constant, the reactivity will be a function of the LUMO energy of the inhibitor, the lower the energy, the more reactive the molecule. Furthermore, with reference to the Arrhenius equation, it is expected that the relative reactivity of these inhibitors with a given nucleophile will depend exponentially on the LUMO energy. Earlier studies of simple substituted quinones do indicate a correlation between reactivity and LUMO energy.^{34,35} Figure 2 shows the frontier orbitals for the unsubstituted quinone derivative **9g**. It can be seen that the LUMO of **9g** has largely π -character and that the most significant part of the orbital density is centered on the quinone ring. Most of our molecular orbital calculations were performed using the semiempirical AM1 method. Since we are comparing relative LUMO values, we felt that high accuracy in these calculations would not be crucial for our purposes. In performing these calculations, we observed a significant dependence of the LUMO energies on the conformations of the inhibitors with respect to rotations of bonds located nearby the quinone ring and with respect to the orientation of some types of quinone substituents. Molecular mechanics calculations indicate that conformations where the NH group joining the quinazolinone and quinone portions of the molecule forms an intramolecular H-bond with one of the quinone carbonyl groups are more favored than alternate conformations lacking this H-bond. Also, this type of conformation is favored

in our binding models of these inhibitors at the active site in VEGFR-2. Accordingly, the conformation we used to calculate the frontier orbitals of **9g** shown in Figure 2 is of this type.

Conceivably, under neutral or physiological conditions, the reaction of a substituted quinone-based inhibitor such as **76** with a sulfhydryl-containing species, either in solution or in the VEGFR-2 enzyme-bound state, can involve a redox process consisting of a one-electron reduction, wherein discrete semiquinone-like intermediates³⁶ such as **77a–c** are formed (Scheme 6). We are assuming that the formation of these intermediates occurs in the rate-determining step of the reaction. These intermediates can be interrelated by tautomerization. As stated above, the propensity to form these intermediates will be a function of the LUMO energy of **76**. These semiquinone intermediates, in turn, can combine with the sulfur radical formed in the reaction or the neutral sulfhydryl species, followed by a subsequent tautomerization, to produce a reductive addition product **A**. Alternatively, when a quinone substituent has the ability to function as a leaving group and the position of attack of the sulfur radical is at the site of the quinone substituent, an ipso substitution product, **B**, can result. Since the ipso substitution product is itself a quinone, further reaction, when in solution, with the sulfhydryl species is possible, resulting in the formation of a bis-adduct **F**. Additionally, in the presence of an excess of reducing species, the semiquinone intermediates **77a–c** or the ipso substitution product **B** can be further reduced to give the hydroquinone products **E** and **C**, respectively. Finally, since the reactions studied were done without protection from atmospheric oxygen and since any quinoid species present can act as an oxidizing agent, the hydroquinone products **A**, **C**, **E**, and **F** can be reoxidized and subsequent addition of a sulfhydryl species could result in multiple addition products such as **G**. Under physiological conditions, it is expected that products of type **C–G** can form only when the inhibitor is unbound, in the circulation or cytosol, but not when the inhibitor is in the enzyme-bound state, since a second reducing group is absent at the active site and there is no oxidizing source to reoxidize a hydroquinone adduct. Therefore, it is expected that the drug–VEGFR-2 conjugate will be a product of either type **A** or **B**, where the SR'' group represents the protein.

The types of products formed and their regiochemistry will be determined in steps after the rate-determining step and will depend on a number of factors, including the relative populations of the semiquinone tautomers and their conformations, the steric influence of the quinone substituents, the ability of a substituent to serve as a leaving group, and the distribution of the orbital density in the singly occupied molecular orbital (SOMO) of the semiquinone intermediates. In the case of the enzyme-bound inhibitor, the relative orientation of the two reacting centers may also be a factor in product formation. To further understand the regiochemistry of this type of reaction, we determined the products resulting from the reaction of some selected inhibitors with simple sulfhydryl-containing nucleophiles (Scheme 6 and Table 1). The mass spectra of the reaction mixtures were monitored over a 24 h period.

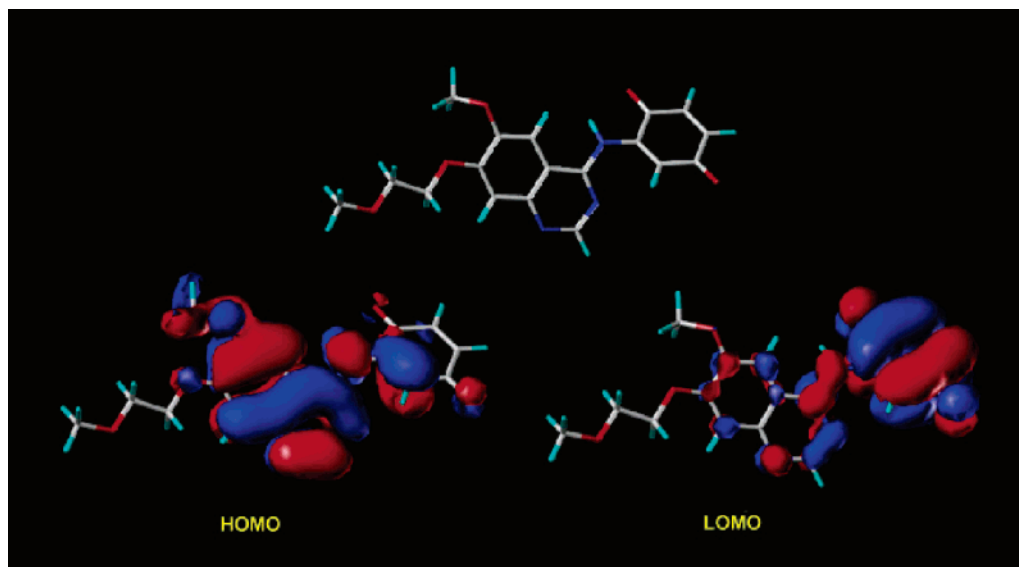


Figure 2. Frontier molecular orbitals of a low-energy conformation of **9g** by the AM1 method using the MOPAC module in Sybyl. Note that the LUMO is largely of π -character and is localized predominately on the quinone ring.

If a mass corresponding to any of the potential products **A–G** was observed in the mass spectrum during this time period, it is so indicated in the table. In some cases the products were isolated and their regiochemistry was determined by NMR. Product ratios varied over time with multiple addition/reoxidation products increasing with time.

Knowledge of the rates of reaction of these quinone-based inhibitors with a sulfhydryl-containing species could be important information that might help in the interpretation of some of our biological observations. Accordingly, we measured the half-life ($t_{1/2}$) of selected 5-substituted inhibitors in the presence of reduced glutathione in H_2O –acetonitrile (1:1). A 1 or 10 μM solution of the inhibitor was incubated in the presence of 100 μM of glutathione, and the amount of inhibitor remaining over time was monitored by HPLC–MS. It is clear from the data shown in Table 2 that the rates of reaction of these molecules are highly dependent on the quinone substituents with $t_{1/2}$ values varying between less than 1 min to weeks long.

Also shown in Table 2 are the calculated LUMO energies for the inhibitors. During preliminary calculations it was evident that, in some cases, the LUMO energies varied significantly between different conformations of the inhibitors. While the LUMO values were usually insensitive to conformational changes at positions remote from the quinone ring (such as the 6- and 7-positions of the quinazoline), the energies were sensitive to rotations of bonds located nearby the quinone ring and to the orientation of certain quinone substituents. Since the kinetic studies were done under pseudo-first-order conditions, it is expected that, for a given compound, the overall rate of reaction will be a combination of the rates of reaction of the individual conformers weighted by their concentration. Similarly, it seems appropriate to express the LUMO energies as weighted averages of the energies of the individual conformers. Accordingly, for the compounds listed in Table 2, we did a full conformational grid search with respect to bond rotations located nearby the quinone ring. For each of these conformers we calculated a LUMO energy. Fi-

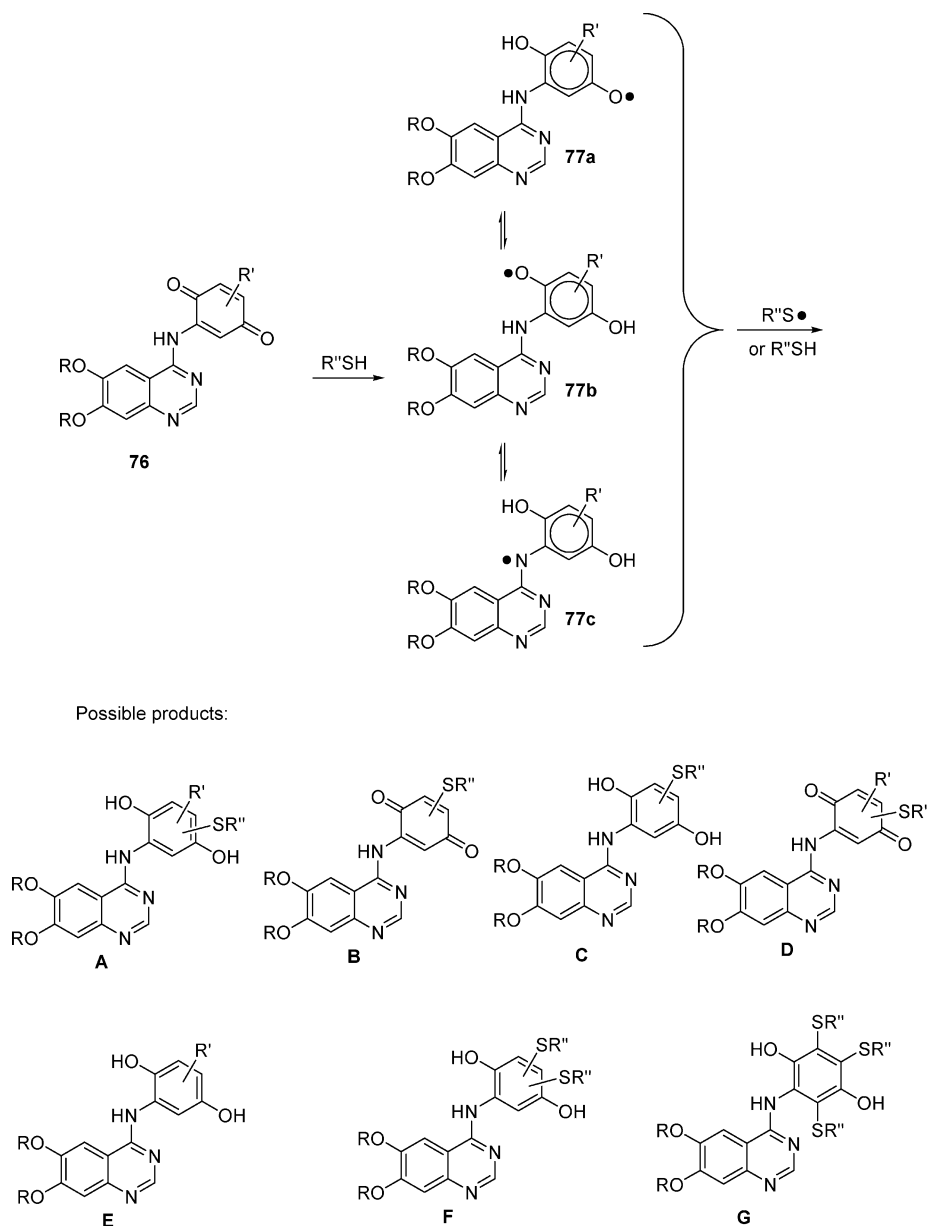
nally, a single LUMO energy value was obtained that was derived from a weighted average of the individual LUMO values on the basis of the Boltzmann distribution of the conformers. In general, we find that electron-withdrawing groups attached to the quinone ring lower the LUMO energy (more reactive) while electron-donating groups raise it (less reactive).

It is evident from the data shown in Table 2 that the reactivities of these inhibitors are correlated with the averaged LUMO energies. The minor discrepancies in the correlation can be attributed to other effects such as those of steric origin and the fact that these calculations are for neutral molecules in the gas phase and certain derivatives such as **23** are expected to be protonated under the reaction conditions. In general, the lower the LUMO energy, the more reactive the molecule appears to be. Moreover, these data suggest that the correlation is not linear but is approximately exponential. We therefore feel that these LUMO values can be useful predictors of the reactivities of these inhibitors and they will be used as such in the discussions to follow.

Molecular Modeling. A binding model for one of our inhibitors, **26**, in the active site of VEGFR-2 is presented in Figure 3. The initial protein coordinates used in these studies are those reported for the crystal structure of the catalytic domain of VEGFR-2.²⁵ Water molecules were removed and the inhibitor was docked using the docking algorithm FRED.³⁷ Low-energy poses were rescored using the Poisson Boltzmann molecular mechanics scoring function (PBMM-SA).³⁸ The resulting model shows the inhibitor oriented in a manner consistent with the way other quinazoline derivatives have been shown to bind to different kinases.^{28,29}

A favorable interaction between the quinazoline N1 of **26** and the hinge region backbone NH of Cys-919 is found to be significant in our model. The polar aromatic hydrogen atom between N1 and N3 of the quinazoline ring is favorably oriented at approximately 3 Å from the backbone carbonyl of Glu-917. In the most favored bound conformation, the oxygen atom of a quinone carbonyl group makes an intramolecular H-bond to the

Scheme 6



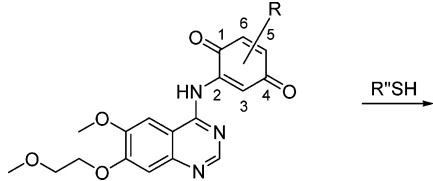
NH substituent on the quinazoline. This is similar to the low-energy conformations found for the unbound inhibitors. The other quinone carbonyl is oriented toward the side chain of Lys-868, within approximately 3.4 Å. The center of the quinone ring is perpendicularly oriented toward the sulfhydryl group of Cys-1045, being located about 4.5 Å away, and is within a distance that should allow covalent bond formation considering thermal motions of the bound inhibitor and the protein. Interactions of quinone substituents with the VEGFR-2 binding pocket will vary, depending on the nature of the substituent and its location on the quinone ring. For **26**, the 1,3-difluoroisopropoxy substituent occupies a region of the binding pocket proximal to the region where Lys-868 and Asp-1046 are found. This region extends into a hydrophobic pocket over 10 Å up toward the N-terminus of the kinase where larger quinone substituents, on the 5-position of the quinone ring, can fit. Thus, lipophilic interactions in this region could result in enhanced protein–ligand binding energetics.

Biology

The results of our biological assays are shown in Table 3. Our primary assay is a DELFIA kinase assay,³⁹ where recombinant full cytoplasmic domain of human VEGFR-2 is utilized and where the activity of an inhibitor is expressed as an IC₅₀. Usually, this assay is conducted using a 10 μM concentration of ATP. For selected compounds, to explore the ATP-competitive nature of the inhibition, the assay was also conducted at a 1 mM ATP concentration.

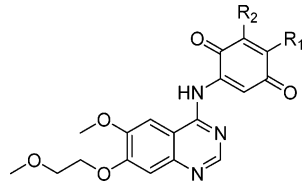
As stated above, since the reactivity of our inhibitors toward sulfhydryl-containing nucleophiles is an important issue, we decided, for selected compounds, to also determine IC₅₀s in the presence of 100 μM concentration of glutathione and in the presence of fresh mouse plasma. It is unlikely that a compound that loses inhibitory activity when tested in the presence of these agents could ever become a useful drug.

While the IC₅₀ of a conventional ATP competitive inhibitor is a direct measure of the compound's ability

Table 1. Observed Products (see Scheme 6) of the Reaction of Selective Inhibitors with a Sulfhydryl-Containing Species^a


compd	R	product type (Scheme 6)						
		A	B	C	D	E	F	G
16^b	5-OMe	+	-	-	-	-	-	-
15^b	5-OCH ₂ Ph	+	-	-	+	-	-	-
13^c	5-OPh	+	+	-	-	+	+	-
26^d	5-OCH(CH ₂ F) ₂	-	+	-	+	-	+	+
9h^e	6-OMe	+	-	-	+	-	-	-
9a^f	5-Cl	+	+	+	-	+	+	-
9l	5-SMe	-	+	-	-	-	-	-

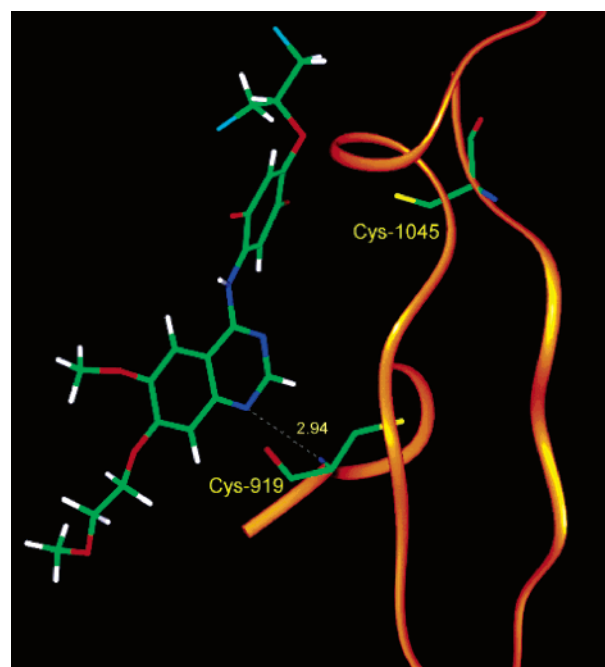
^a Reactions were conducted under air in CH₃CN/H₂O or THF/MeOH/H₂O solutions with the sulfhydryl species in excess (4–10-fold). Reactions were analyzed at various time points by HPLC–MS or by measuring the MS of the mixture directly. A + sign indicates observation of the designated product, while a – sign indicates that it was not observed at the time of the measurement. Minor products have a + sign. Unless indicated otherwise the sulfhydryl nucleophile was ethylmercaptan. ^b The regiochemistry of **A** was 5-OR-3-SR' as shown by NOE. ^c The sulfhydryl nucleophile was glutathione. The regiochemistry of the products were not determined. ^d The regiochemistry of **D** was 5-OCH(CH₂F)₂-3-SR' as shown by NOE. The oxidized forms of **F** and **G** were observed. ^e The regiochemistry of the products is suggested to be 6-OMe-3-SR' in analogy to **9j**. ^f The regiochemistry of **A** and **F** was not determined.

Table 2. Half-Life (*t*_{1/2}) of Selected Compounds at 1 and 10 μM Concentrations in the Presence of 100 μM of Glutathione in H₂O–Acetonitrile (1:1)^a and the Calculated LUMO Energies^b


compd	R ₁	R ₂	<i>t</i> _{1/2} (h)		LUMO ^b (eV)
			10 μM	1 μM	
9a	Cl	H	<0.02	<0.02	-1.92
13	OPh	H	<0.02	<0.02	-1.82
18	OPh-4-N-imidazolyl	H	<0.02	<0.02	-1.78
9c	OCH ₃	Cl	0.5	<0.5	-1.89
9l	SCH ₃	H	3	2	-1.81
26	OCH(CH ₂ F) ₂	H	15	11	-1.80
15	OCH ₂ Ph	H	54	55	-1.68
36	OCH ₂ CH ₃	H	72	62	-1.52
16	OCH ₃	H	80	68	-1.54
23	N-piperazinyl-4-CH ₂ Ph	H	85	73	-1.59
29	OCH(CH ₃) ₂	H	227	213	-1.48
12	N(CH ₃)Ph	H	295	341	-1.62
10	N(CH ₃) ₂	H	601	160	-1.51

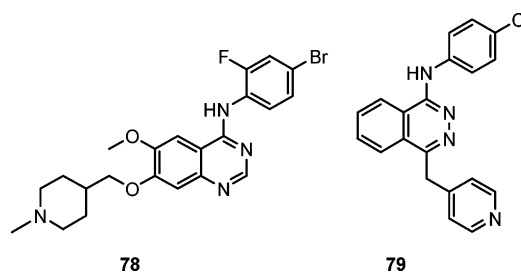
^a Kinetic studies were conducted at room temperature in air. ^b LUMO energies are averages of those of individual conformers weighted by the Boltzmann distribution.

to fit at the active site and compete with ATP, the situation is expected to be more complicated for an irreversible binding inhibitor where the IC₅₀ will be a measure of both the fit at the active site as well as the reactivity of the molecule. In this situation, one expects that for two molecules that fit the site equally well, the more reactive molecule will have a lower IC₅₀. The IC₅₀ value that we measure for a covalent-binding inhibitor could be time-dependent and additionally, depending on

**Figure 3.** Binding model for **26** at the active site of VEGFR-2. Protein coordinates are those from the reported crystal structure. The distance of the sulfur atom of Cys-1045 from the center of the quinone ring is about 4.5 Å.

the rate of reaction of this type of inhibitor with the target enzyme, the IC₅₀ value could simultaneously consist of components reflecting both reversible and irreversible binding.

For comparison, enzyme data for the known reversible-binding ATP-competitive inhibitors, the quinazoline **78** (ZD4190)⁴⁰ and the phthalazine **79** (PTK787),⁴¹ are included in Table 3.



In addition to the aforementioned enzyme assays, we evaluated these inhibitors in KDR15 cells (human embryonic kidney 293 cells transfected with full length VEGFR-2),⁴² where we measured the inhibition of VEGF-stimulated VEGFR-2 autophosphorylation. Again, the measurement is expressed as an IC₅₀ value.

Also included in Table 3, as predictors for reactivity, are the calculated LUMO energy values. While the LUMO values for those compounds given in Table 2, calculated from the Boltzmann distribution of the conformers, are repeated in Table 3, the majority of the LUMO values in Table 3 were not derived from the Boltzmann distribution but, instead, are calculated for single minimized conformations. The conformations used in the calculation are low in energy and each has the intramolecular H-bond, between the quinone carbonyl group and the NH group with the quinazoline–

Table 3. Inhibition of VEGFR-2 Kinase, Inhibition of VEGF-Stimulated VEGFR-2 Autophosphorylation in KDR15 Cells, and LUMO Energies

compd	IC ₅₀ (nM)					LUMO (eV) ^f	compd	IC ₅₀ (nM)					LUMO (eV) ^f
	10 μM ATP ^a	100 μM GSH ^b	5% plasma ^c	1 mM ATP ^d	KDR15 cells ^e			10 μM ATP ^a	100 μM GSH ^b	5% plasma ^c	1 mM ATP ^d	KDR15 cells ^e	
9a	4.4	>1000	569.1		>1000	-1.90 (-1.92)	31	<1	6.8				-1.96
9b	13.5					-2.00	32	<1	21.3			>1000	-1.87
9c	1	20.9	5.1	<1	466	-1.70 (-1.89)	33	52.4	70	>1000			-1.62
9d	67.1	>1000	>1000			-1.90	34	31.2	41.9	256.3			-1.60
9e	1.7	>1000	375.9			-1.91	35	23.6	32.7	239.2		>1000	-1.65
9f	109.4			607.8	<15	-1.65	36	>1000	>1000	>1000		>1000	-1.56 (-1.52)
9g	6				>1000	-1.64	37	4.6	365.9	57.4		>1000	-1.69
9h	3.8					-1.64	38	5.8	18.6	495.2			-1.71
9i	111.9					-1.90	39	4.5	25.2	32.5		870	-1.74
9j	>1000	>1000	>1000			-1.69	40	3.4	8.1	16.5			-1.61
9k	15.8	881.6	803.1			-1.91	41	>1000	>1000	>1000			-1.43
9l	30.1	>1000	114.7	43.3	456	-1.80 (-1.81)	42	10.3	>1000	59.7	7.3	>1000	-1.71
9m	9	>1000	>1000			-1.92	49	16.1	>1000	28.7			-1.77
10	1144.1	5000.3	>20000		31	-1.38 (-1.51)	50	5.7	>1000	41			-1.96
11	101.2				>1000	-1.49	51	2.3	>1000	193.5			-1.91
12	16	>1000	>1000		>1000	-1.45 (-1.62)	52	1.9	>1000	97.3			-1.87
13	2.7	>1000	560.1		184	-1.75 (-1.82)	60	239.3	239.7	129.9	3020.7	5	-1.53
14	236.5	474.4				-1.71	61	5.1	6.9	3.7	11.2	189	-1.62
15	43	50.3	366.1			-1.59 (-1.68)	62	3.9	15.3	5.8		329	-1.53
16	240.9	558.6	>1000	436.3	25	-1.59 (-1.54)	63	13.6	29.5	26.1		536	-1.55
17	359.4	>1000			310	-1.41	64	271.8	406.3	158.6	1274	3	-1.58
18	7.6	>1000	>1000	5.8	310	-1.91 (-1.78)	65	6.4	12.8	7.4			-1.81
19	0.9					-1.75	66	1.5	1.8	1.9	1.7		-1.73
20	2.6				78	-1.55	67	9.6	15.1	2.2			-1.68
21	540.2	>1000			206	-1.71	68	16.9	31.8	13.7			-1.54
22	298.6	231.8	>1000			-1.35	69	4.5	6.3	9.9			-1.71
23	84.8	125.4	>1000	75.5	>1000	-1.58 (-1.59)	70	3.6	8.8	5.2	10.4		-1.67
24	133	270.6	>1000		>1000	-1.42	71	5.1	9	4.8			-1.71
25	371.9	>1000	>1000			-1.33	72	70.7	83.1	53.5			-1.66
26	9.1	21.3	24.8	18.5	212	-1.89 (-1.80)	73	35.9	42.1	29.6			-1.69
27	88.7	110.5	>1000	107.8	193	-1.66	74	4.2	5.1	13.9			-1.53
28	1.7	4.8	117.8		>1000	-1.64	75	3.2	18.3	2.4			-1.8
29	491.3	>1000	>1000	542.9	481	-1.54 (-1.48)	78	41.8	31.3	149.8	5980.5	<15	
30	0.4	70.9	3		792	-2.07	79	138			6308.1	<15	

^a The assay was conducted using an ATP concentration of 10 μM. The IC₅₀ is the concentration in nM needed to inhibit the phosphorylation of the poly(Glu₄-Tyr) peptide by 50% as determined from the dose-response curve. Where there were multiple determinations, the IC₅₀ values were averaged, and the standard deviations, on average, were 43% of the average IC₅₀ value. ^b The assay was conducted in the presence of 100 μM of glutathione using an ATP concentration of 10 μM. Where there were multiple determinations, the IC₅₀ values were averaged, and the standard deviations, on average, were 39% of the average IC₅₀ value. ^c The assay was conducted in the presence of 5% (v/v) fresh mouse plasma using an ATP concentration of 10 μM. Where there were multiple determinations, the IC₅₀ values were averaged, and the standard deviations, on average, were 41% of the average IC₅₀ value. ^d The assay was conducted using an ATP concentration of 1 mM. Where there were multiple determinations, the IC₅₀ values were averaged, and the standard deviations, on average, were 29% of the average IC₅₀ value. ^e Concentration in nM needed to inhibit the VEGF-stimulated autophosphorylation VEGFR-2 in intact KDR15 cells by 50% as determined from the dose-response curve. Where there were multiple determinations, the IC₅₀ values were averaged, and the standard deviations, on average, were 42% of the average IC₅₀ value. ^f LUMO values calculated by the AM1 method using MOPAC as implemented in Sybyl for a single low-energy conformation similar to that as shown in Figure 2. LUMO energies in parentheses are averages of those of the individual conformations weighted by the Boltzmann distribution.

NH-quinone torsional angles similar to those shown in the structure in Figure 2. Conformations of this type are energetically favored and favored by our binding models. However, an arbitrary, but minimized, orientation was used for the quinone substituents. With the possible exception of some of the compounds with conformationally mobile quinone substituents having multiple heteroatoms or those compounds where rotations along the quinazoline-NH-quinone torsional angles result in large changes in the location of polar or conjugated substituents, these LUMO values should approximate those obtained by utilizing a full conformational analysis. However, due to the uncertainties resulting from not evaluating these LUMO energies using a complete conformational analysis, these LUMO energies should only be viewed as rough estimates for the reactivities.

With respect to the conventional reversible binding inhibitors **78** and **79**, each is a moderately potent

inhibitor in our VEGFR-2 enzyme assay. The quinazoline-based inhibitor **78** was studied in detail and it is evident that it retains full activity when tested in the presence of glutathione. It loses some (2–3-fold) activity when tested in the presence of plasma, possibility due to protein binding. Both **78** and **79** show good potency in our cell-based autophosphorylation assay. These results will serve as a basis with which to compare reversible-binding ATP-competitive inhibitors with our quinone-based irreversible binding inhibitors.

Among the more potent enzyme inhibitors are those that have an electron-withdrawing halogen substituent at the 5-position of the quinone ring, such as **9a** and **9m**. As indicated by the short half-life observed in the kinetic experiment with **9a** and suggested by the very low LUMO energies calculated for these derivatives, these 5-halo substituted compounds have high reactivity. It is therefore not surprising that they lose a significant part of their inhibitory activity when tested

in the presence of glutathione or plasma. One of these derivatives, **9a**, was evaluated in the cell-based phosphorylation assay and was found to be inactive. Presumably, as a result of its high reactivity, **9a** is scavenged by endogenous nucleophiles within the cell before it gets a chance to reach the target enzyme. As one might expect, the addition of a second Cl atom, to give the 5,6-dichloro derivative **9b**, decreases the LUMO energy further with retention of good potency in the enzyme assay. Placement of an electron-releasing alkoxy group at the 6-position, as in compounds **9e**, **51**, and **52** does not significantly overcome the influence of the 5-chloro substituent, both with respect to the calculated LUMO energies and the biological properties of the molecules.

Like the 6-alkoxy-5-chloro analogues, the 5-alkoxy-6-chloro derivatives such as **9c** and **32** are very potent inhibitors of VEGFR-2. However, in contrast to the former series, these inhibitors tend to retain good activity when tested in the presence of glutathione or plasma, despite their low LUMO energies (compare the isomers **9c** and **9e**). The 6-alkoxy-3-chloro derivative **9i**, which is isomeric with both **9e** and **9c**, is a significantly less potent inhibitor (64–110 fold) than either of the other isomers, despite the fact that the calculated LUMO energies for **9e**, **9c**, and **9i** are about the same. In this case, it is likely that the relative potency of these isomers is significantly influenced by other factors in addition to reactivity. It is possible that the presence of a 3-substituent prevents the inhibitor from adopting an appropriate binding conformation by forcing the quinazolin-NH-quinone torsional angles into a less than ideal arrangement. Indeed, none of the inhibitors we prepared that have 3-substituents, such as **9d** and **9j** (and others not shown), have high potency. Another example of the influence of a 3-substituent can be seen in comparing the activities and LUMO energies of **9d** and **9c**.

Another group of inhibitors that generally showed high potency in the enzyme assay and high reactivity are the derivatives with 5-phenoxy-substituted quinones such as **13** and **18–20**. The kinetic experiment (Table 2) with **18** clearly illustrates its high reactivity. While the calculated LUMO energies are not as low as those obtained for the halogen-substituted quinone derivatives, the energies are still well below those calculated for simple alkoxy-substituted compounds. For those cases (**13** and **18**) where we performed the enzyme assay in the presence of glutathione or plasma, the compounds lost most of their activity. Again, we attribute this to the instability of the compounds in the presence of reducing species. Nevertheless, some of these compounds do have activity in the cell autophosphorylation assay with IC₅₀ values in the sub- μ M range, suggesting that the relative reactivity of these analogues, in cells, with the VEGFR-2 target is competitive with that of any endogenous reducing species.

Among the inhibitors we prepared, those with an alkylamino substituent on the quinone ring, such as **10**, **11**, **17**, and **21–25**, are predicted to be the least reactive. The alkylamino groups are the strongest electron-donor groups that we incorporated onto our inhibitors, and the calculated LUMO energies for these compounds are among the highest found. In particular, the 5-dimethylamino derivative **10** is the least reactive molecule we

found in our kinetic experiments (Table 2). Perhaps reflecting this low reactivity is the low potency exhibited by this and related compounds in our enzyme assay. While several of these amino-substituted derivatives such as **22–24** appear to retain much of their activity when tested in the presence of glutathione, it is not clear whether these compounds are functioning entirely as covalent-binding inhibitors, and in fact, they may partly function as conventional reversible binding inhibitors over the short time course of the enzyme experiment. The relatively high IC₅₀ values would then simply reflect a less than optimal fit at the active site. Among the alkylamino-substituted inhibitors that have been evaluated in our cell-based autophosphorylation assay, some, such as **10**, **17**, and **21**, show inhibitory activity comparable to that observed in the enzyme assay.

The derivative **42**, having a cyclic urethane moiety at the 5-position of the quinone ring, showed a significant increase in potency relative to the alkylamino-substituted inhibitors in the enzyme assay. One could anticipate that the electron-donating ability of the urethane N-atom would be greatly attenuated relative to that of an ordinary dialkylamino group and this appears to be reflected in the calculated LUMO energy of **42**, which has decreased significantly compared to that found for the alkylamino-substituted derivatives. It is likely that the increase in potency observed for **42** is due, in part, to its increased reactivity. Additionally, this increased reactivity of **42** could be a controlling factor resulting in a loss of its activity in the enzyme assay when tested in the presence of glutathione, and it may be responsible, in part, for the lack of activity in the cell assay.

The inhibitor incorporating an *N*-methylaniline moiety at the 5-position of the quinone ring, **12**, proved to be a good inhibitor of VEGFR-2 with an IC₅₀ = 16 nM. However, the compound lost activity when tested in the presence of glutathione, despite the fact that the kinetic experiment (Table 2) suggested that this compound is only a moderately reactive substance.

An example of an inhibitor with a sulfur atom attached to the 5-position of the quinone ring was prepared, the methylthio derivative **9l**. On the basis of the LUMO energy, it is predicted to be fairly reactive, and this was confirmed by the kinetics exhibited by the compound (Table 2). The compound showed good potency in the enzyme assay, but it did not retain its activity when tested in the presence of glutathione.

One group of compounds that we extensively studied comprises inhibitors having an alkoxy substituent at the 5-position of the quinone ring. The LUMO energies that we calculate for inhibitors with simple alkyl groups fall within the midrange of the LUMO scale. Additionally, we found that we could modulate the LUMO energies by altering the substituents attached to the alkoxy group. We observed an interesting trend with respect to the methoxy-substituted derivatives **16**, **60**, and **64**. While these compounds are only moderately potent inhibitors in our enzyme assay, they are among the most potent inhibitors in our cell-based autophosphorylation assay. In fact, for these compounds, the IC₅₀ values for inhibiting VEGFR-2 autophosphorylation in intact cells is lower than that observed for inhibiting the enzyme in solution. A truly satisfying explanation for this observation is lacking, but one can speculate that these

compounds are more efficient inhibitors of the full-length, membrane bound, enzyme present in cells compared to the truncated cytoplasmic domain used in the enzyme assay, and in fact, in an earlier study²⁷ with EGFR, we observed such a situation where IC₅₀ measurements were higher with a truncated enzyme compared to the full length enzyme. On the basis of the kinetic experiments (Table 2), the simple alkoxy derivatives **16**, **29**, and **36** are only moderately reactive. Nevertheless, as will be discussed below, mass spectral studies do prove that one of these compounds, **16**, does indeed form a covalent interaction with the enzyme. The moderate reactivity of these compounds could also be a factor contributing to the improved cell activities. Compared to the 5-methoxy analogues, those having isopropoxy or ethoxy substituents, **29** and **36**, respectively, are less potent in the enzyme assay, even though they have similar LUMO energies.

Intuitively, one might have expected that adding an additional electron-donating methoxy group to the 6-position of the quinone to give the 5,6-dimethoxy derivative **49** would have resulted in a molecule having a higher LUMO energy and decreased reactivity, but in fact, this additional methoxy group results in a lowering of the LUMO energy. This could be a contributing factor in the greater potency of **49** compared to **16** in the enzyme assay.

We prepared a number of compounds where the 5-alkoxyquinone substituent has an attached unsaturated and lipophilic group, for example, the 5-benzyloxy-substituted derivatives **15**, **33–35**, **38**, **63**, **68**, and **69**. On the basis of the weighted average LUMO energies calculated for the benzyloxy analogue **15** and for the simple alkoxy derivatives **16**, **29**, and **36**, it appears that the benzyloxy group contributes to a lowering of the energy. Thus, compared to these simple alkoxy-substituted derivatives, **15** is predicted to be more reactive. The kinetic experiments do confirm this, although the differences in reactivity are modest. These benzyloxy derivatives are clearly more potent than the simple alkoxy analogues. A combination of higher reactivity and an improved fit at the active site for the benzyloxy-substituted inhibitors could account for the improved potency. To be sure, our binding model for these inhibitors indicates that there is a large lipophilic pocket that could easily accommodate a benzyloxy group, resulting in an improved interaction with the enzyme. Interestingly, each of these benzyloxy-substituted inhibitors retains a significant portion of the enzyme activity when tested in the presence of glutathione and, in some cases, in the presence of plasma as well. The related heterocyclic analogues **27**, **67**, and **74** show an in vitro profile similar to that of the benzyloxy substituted inhibitors. The inhibitor **31**, which has a 6-chloro group on the quinone ring in addition to the 5-(*m*-fluorobenzyloxy) group, is an extremely potent inhibitor of VEGFR-2, even in the presence of glutathione, although the calculated LUMO energy suggests that it should be a very reactive molecule.

Additional inhibitors that have unsaturated and lipophilic oxy substituents at the 5-position of the quinone ring, such as **28**, **40**, **62**, **66**, and **70–73**, are also potent VEGFR-2 inhibitors with IC₅₀ values in the range 1.5–70 nM, and almost all of these compounds

retain their activity when tested in the presence of glutathione or plasma. The LUMO energies calculated for these compounds suggest intermediate reactivity.

A most interesting group of inhibitors are those that have a fluoroalkoxy group attached at the 5-position of the quinone ring. These inhibitors include **26**, **30**, **50**, **65**, and **75**. MO calculations indicate that the strong inductive electron-withdrawing nature of the fluorine atoms can result in a significant lowering of the LUMO energies. Calculated LUMO energies for these inhibitors were very sensitive to the overall orientation of the fluoroalkyl group and to the relative orientation of the fluorine atoms within the group. In particular, for the 1,3-difluoroisopropoxy-substituted compounds, we found that LUMO energies could vary more than 0.3 eV between low-energy conformers having different relative orientations of the two fluorine atoms. Because of this, the LUMO energies calculated from the weighted averages of the conformations should be considered more reliable than those calculated from single conformations. By comparing compounds **26** and **29**, having the sterically similar 1,3-difluoroisopropoxy and isopropoxy groups attached to the quinone ring, respectively, one can see the striking influence the fluorine atoms have on reactivity (Table 2). The fluorine atoms lower the LUMO energy of **26** by over 0.3 eV compared to **29**. The result of this is the very significant decrease in the *t*_{1/2} of **26** compared to **29**. The enhanced reactivity of **26** likely accounts for its greater potency in the enzyme assay compared to **29**. In addition, much of the activity is retained for **26** when the assay is conducted in the presence of glutathione or plasma. The increased potency for **26** compared to **29** is also evident in the cell assay, but it is not as impressive.

It is well-established for the quinazoline and the related 3-cyanoquinoline-based kinase inhibitors that placement of a water-solubilizing substituents at the 6- or 7-position results in improved solubility and bioavailability. Binding models for these types of compounds indicate that such water-solubilizing groups point out toward solvent, and therefore, we expected that incorporation of a water-solubilizing substituent at the 7-position in our series would have a minimal effect on the potency of these inhibitors in our enzyme assay. For the most part, this is what we observed. For example, compare the triplets of compounds with benzyloxy substituents (**15**, **63**, and **68**), methoxy substituents (**16**, **60**, and **64**), and 1,3-difluoroisopropoxy substituents (**26**, **61**, and **65**), where in each trio, the side chain at the 7-position of the quinazoline is altered. In each case, there is a minimal change in the enzyme inhibitory activity resulting from altering the side chain.

Since the molecules discussed herein are reactive, one might wonder whether they will lack selectivity by acting as indiscriminant alkylators of other kinases. In fact, this appears not to be the case. Two compounds of moderate reactivity, **60** and **61**, were evaluated against a panel of other kinases consisting of AKT, BTK, CDK4, EGFR, GSK, IGFR, IKK, ITK, LCK, LYN, Mek, MK2, mTor, PDK1, PI3K, PKC- θ , and Tpl2. In these assays, IC₅₀ values for **60** varied between 2.2 and >200 μ M and those for **61** varied between 1.8 and >117 μ M. For both compounds, in the majority of the assays (14 out of 17), the IC₅₀ values were ≥ 10 μ M. While for each compound,

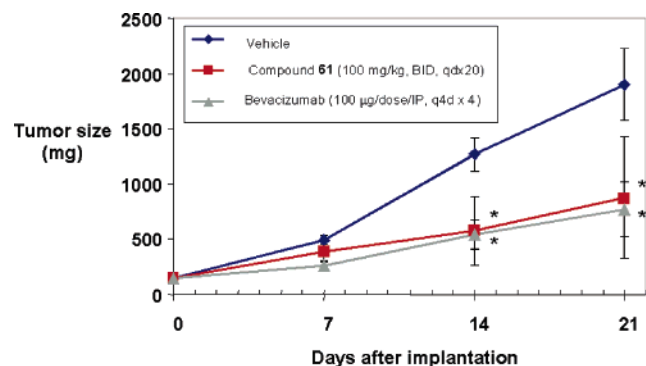


Figure 4. The effect of **61** on the growth of DLD1 cells implanted into athymic mice and staged to ~100 mg. Mice were treated with 100 mg/kg of **61** (po/b.i.d.), vehicle (Methocel/Tween, po/b.i.d.) or 100 μ g/dose bevacizumab (anti-VEGF antibody, ip, days 1, 5, 9, 13). Relative tumor growth was determined every 7 days for a period of 21 days. Data are the mean fold increase in tumor volume in each group. * $p \leq 0.05$ by Student's *t*-test.

low μ M activity was observed in inhibiting LCK and PI3K, **60** was still 5–6 times more potent and **61** was 120–500 times more potent in inhibiting VEGFR-2 compared to LCK and PI3K, respectively. In many of the above assays, thiol reagents were used as part of the buffer mixture. It is therefore not entirely clear what influence these thiol reagents may have had on these selectivity measurements.

In Vivo Efficacy. We selected **61** for in vivo evaluation since it is a potent inhibitor of the enzyme that also retains activity when tested in the presence of glutathione or plasma and has reasonable potency in the cell-based assay. Additionally, the kinetic experiments with the related quinone **26** suggest it may have a useful half-life in circulation. The compound was evaluated in a nude mouse xenograft model bearing the human colon carcinoma DLD1. The results are shown in Figure 4. For comparison, data are also shown for the VEGF antibody bevacizumab. The inhibitor was administered, at the indicated dose, orally twice daily for the first 20 days of the experiment. Bevacizumab was dosed ip every fourth day. It is evident that oral administration of **61** results in a statistically significant reduction in tumor growth. Relative to the control animals, there was a 54% reduction in the tumor mass after 20 days of dosing. The efficacy of **61** in this experiment was comparable to that exhibited by bevacizumab.

Evidence for Covalent Binding. We have accumulated a body of evidence that strongly suggests that these quinone-based inhibitors bind irreversibly to VEGFR-2 kinase. For example, these compounds appear to behave as non-ATP-competitive inhibitors, as shown by the data given in Table 3, where we compared our inhibitors with the known conventional ATP-competitive inhibitors **78** and **79**. One would expect, for an ATP-competitive inhibitor, that the IC_{50} value for inhibition would increase when the concentration of ATP is increased. The data presented in the table for **78** and **79** clearly indicate that this is so; the IC_{50} values increased 142- and 45-fold, respectively, when changing the ATP concentration from 10 μ M to 1 mM. In contrast, when our inhibitors were tested at the two ATP concentrations, the increase in the IC_{50} values, on average,

Table 4. MALDI Mass Spectral Results for Incubation of **16** and **18** with VEGFR-2^a

compd	obsd mass (Da)	D mass (Da)	no. of molecules
VEGFR-2	63 897		
18	65 112	1215	2.3–3.4
16	64 462	565	1.2

^a VEGFR-2 was incubated with a 10-fold excess of the inhibitor for 1 h.

Table 5. HPLC-ESI Mass Spectral Results from a Time Course Study of **16** Incubated with VEGFR-2 over a 20-h Period^a

incubation time (h)	obsd mass (Da)	D mass (Da)	no. of molecules
0	64 134 \pm 31		
2.5	64 608 \pm 79	475	1.2 \pm 0.22
5	64 896 \pm 70	763	2.0 \pm 0.20
20	64 845 \pm 49	712	1.9 \pm 0.15

^a VEGFR-2 was incubated with a 10-fold excess of **16**.

was only about 2-fold, and for some compounds, the increase was negligible. This is exactly the result one would expect for an irreversible inhibitor of the enzyme.

Additional, more definitive, evidence that our compounds are functioning as covalent-binding inhibitors of VEGFR-2 kinase was gathered from mass spectral studies, where the VEGFR-2 protein was incubated with the inhibitors **18** and **16**, the former representing the very reactive and the latter representing the moderately reactive types of inhibitors. In addition to VEGFR-2, we utilized the proteins BSA and HSA as controls. Table 4 summarizes the results of MALDI-MS studies with these compounds. The MALDI mass spectrum of our sample of the intracellular domain of human VEGFR-2 showed a broad peak corresponding to a protein with a mass of 63 897 Da. Incubation of VEGFR-2 with a 10-fold excess of the reactive inhibitor **18** for 1 h resulted in the mass increase shown in Table 4. Depending on whether the alkylations of the protein resulted from reductive addition and/or ipso-substitution (products **A** and/or **B** in Scheme 6), the observed mass increase corresponds to 2.3–3.4 inhibitor molecules being added to the protein mass. We found that **18** also reacted with the control proteins BSA and HSA, as determined from the mass spectra. Evidently, **18** was indiscriminate in its reactions with sulfhydryl groups, as was evident by its reaction at multiple sites on the target VEGFR-2 protein and its reaction with the proteins BSA and HSA, which presumably do not have a true binding site for the inhibitor.

In contrast, the more moderately reactive inhibitor **16** was more discriminating. In the MALDI experiment, we observed, after 1 h incubation with VEGFR-2, a mass increase corresponding to the addition of 1.2 molecules, assuming reductive addition (product **A** in Scheme 6). Additionally, we found that **16** did not react with the control proteins BSA or HSA, as determined from the mass spectra.

We also studied the reaction between an excess of **16** and VEGFR-2 by HPLC-ESI-MS as a function of time. While the protein peaks showed poor resolution, we still were able to extract the data shown in Table 5. These data suggest that there may be up to two molecules of **16** reacting with VEGFR-2 over a 5 h incubation period. Extending the incubation time beyond 5 h resulted to

no further increase in the mass of the protein. While one might expect that the target Cys residue (Cys-1045) is the first to react, we have not performed an additional, better time-resolved, kinetic experiment to determine if the two alkylations occur at different rates (however, see the trypsin digestion experiment below). It is interesting to note that the rate at which **16** reacts with VEGFR-2, in these mass spectral experiments, appears to be significantly faster than the rate at which it reacts with a large excess of glutathione (Table 2), suggesting that the anticipated increase of the reaction rate, due to the entropic effect of binding at the active site, may be operative.

To identify the reacting Cys residues, we performed trypsin digestion experiments. Digestion of our VEGFR-2 sample with trypsin followed by HPLC-MS resulted in the identification of the T37 fragment, as singly and doubly charged ions at 894.5 and 447.7 *m/z*, respectively, corresponding to the predicted fragment containing Cys-1045 with molecular weight of 893.5 Da. In a parallel experiment, VEGFR-2 was first incubated overnight with a 10-fold excess of **16**. Most of the excess drug was removed using ultrafiltration and the resulting isolate was digested with trypsin. Again, the fragment corresponding to T37 was identified, but this time two ions were observed at 1277.6 and 639.3 *m/z*, corresponding to singly and doubly charged ions with a molecular mass of 1276.6 Da. The mass difference between these T37 fragments is consistent with the reductive addition of a molecule of **16** (product **A** in Scheme 6) to VEGFR-2 followed by a reoxidation to the quinone (product **D** in Scheme 6) due to the manipulations being carried out in air. The exact mass measurement for the doubly charged ion was consistent with the proposed elemental composition for the oxidized T37-**16** covalent complex. These results supply definitive evidence that **16** forms a covalent product with VEGFR-2 and that the most significant target residue is Cys-1045. Furthermore, by analogy to the observed solution chemistry of **16** (Table 1), we would predict that the inhibitor is attached to VEGFR-2 via the 3-position of the quinone ring.

The trypsin digestion experiment also showed weak signals in the mass spectrum corresponding to alkylated T45, the trypsin fragment predicted to contain Cys-1116. No other alkylated trypsin fragments were observed. The X-ray structure of the catalytic domain of VEGFR-2 shows that Cys-1116 resides in a shallow pocket located near the surface of the protein with the sulfhydryl group pointing outward, and it should therefore be accessible to an electrophile in solution. The ratio of the ion counts for the T37 and T45 fragments before the reaction with **16** was 0.312. After the reaction, the ratio of the ion counts for the alkylated fragments was about 46, suggesting that **16** reacts significantly faster with the active site Cys-1045 than it does with Cys-1116.

Experimental Section

Expression of Recombinant VEGFR-2 Kinase. The human VEGFR-2 cytoplasmic domain (from Val-805 to Val-1356) was cloned by PCR from first-strand human placental cDNA (Invitrogen), subcloned into pAcGHLT-B (Pharmingen), and expressed in Sf9 cells. GST-His-VEGFR-2 was purified from Sf9 cells by sequential chromatography on NiNTA, HiQ

anion exchange, GSH-affinity, another HiQ anion exchange, and G3000 sizing columns. VEGFR-2 domain was cleaved from N-terminal GST-His with thrombin. VEGFR-2 purity was ~90% (MALDI-MS).

VEGFR-2 Kinase Assay. The kinase activity of recombinant VEGFR-2 was evaluated using a DELFIA (dissociation-enhanced lanthanide fluorescent immunoassay) (Perkin-Elmer Life Sciences) essentially as described previously.³⁹ Specifically, Nunc Maxisorb 96-well plates were coated at room temperature for 1–2 h with 100 μ L per well of 25 μ g/mL poly-(Glu₄-Tyr) peptide (Sigma) in Tris-buffered saline (TBS) (25 mM Tris pH 7.2, 150 mM NaCl). Unbound peptide was washed three times with TBS. The cytoplasmic domain of VEGFR-2 enzyme was diluted (depending on the specific activity of the batch, from 10- to 20-fold) in 0.1% BSA/4 mM HEPES. A master mix of enzyme plus kinase buffer was prepared: (per well) 10 μ L of diluted enzyme, 10 μ L of 5 \times kinase buffer (5 \times = 20 mM HEPES, pH 7.4, 5 mM MnCl₂, 100 μ M Na₃VO₄), and 9 μ L of water. Master mix (29 μ L) was added to each well, and compounds (1 μ L) prepared in 100% dimethyl sulfoxide (DMSO) were added to appropriate wells. Test compounds were added as 50 \times stocks as necessary for single point or dose-response analyses. Controls were done by adding DMSO alone, i.e., no test compound, to wells containing the master mix of enzyme plus kinase buffer. After 15 min at room temperature, ATP/MgCl₂ (20 μ L of 25 μ M ATP, 25 mM MgCl₂, 10 mM HEPES, pH 7.4) was added to each well to initiate the reaction. Final concentrations of the assay components were 10 μ M ATP, 10 mM MgCl₂, 1 mM MnCl₂, 4 mM HEPES, pH 7.4, 20 μ M Na₃VO₄, 20 μ g/mL BSA, 2% DMSO. After 40 min at room temperature, the liquid was removed, and plates were washed three times with TBST (TBS with 0.05% Tween-20). The wells were then incubated for 1 h at room temperature with 75 μ L of ~0.1 μ g/mL europium-conjugated anti-phosphotyrosine antibody (PT66; Perkin-Elmer) prepared in assay buffer (Perkin-Elmer). Plates were washed three times with TBST and then incubated for 15 min in the dark with 100 μ L of enhancement solution (Perkin-Elmer). Plates were read in a Victor-V multilabel counter (Perkin-Elmer) using the default europium detection protocol. Percent inhibition or IC₅₀ values of compounds were calculated by comparison with DMSO-treated control wells. The results are shown in Table 3.

In addition to the conventional assay, the assay was conducted in the presence of 100 μ M of glutathione (Sigma) or 5% (v/v) fresh mouse plasma using the above conditions. For the ATP competition experiments, the assay was conducted as above except that a final concentration of 1 mM ATP was used.

Inhibition of VEGFR-2 Autophosphorylation in Cells.

Human embryonic kidney 293 cells were transfected with full length VEGFR-2 and designated KDR15 cells.⁴² Cells were maintained in 10% fetal calf serum (FCS) in DMEM (Life Technologies), penicillin/streptomycin, plus 0.4 μ g/mL puromycin. Cells were plated in 24-well dishes (approximately 4000 cells per well) and allowed to adhere for 1 day. Compounds prepared in DMSO were diluted into serum-free DMEM media at appropriate final concentrations. Growth media was aspirated from each well, cells were washed with serum-free DMEM, and replaced with 0.5 mL of compound-containing serum-free media. Cells were incubated for 1 h on ice and then 55 μ L of 500 ng/mL VEGF (final concentration 50 ng/mL; VEGF₁₆₅, R&D Systems) was added to each well and the mixture incubated for 30 min on ice. Cells were resuspended during VEGF incubation, transferred to 1.5-mL tubes, and then centrifuged at 12 000 rpm for 10 min. Pellets were lysed in 50 μ L of NP40 lysis buffer (150 mM NaCl, 50 mM Tris, pH 7.5, 2 mM EDTA, 1% NP-40 [Ipegal CA-630], 1 mM Na₃VO₄, 1 mM PMSF, 20 KIU/mL aprotinin, 1 μ g/mL pepstatin, 0.5 μ g/mL leupeptin). Lysates were centrifuged for 10 min at 12 000 rpm at 4 °C and the supernatants transferred to fresh tubes and frozen until use. Equal volumes of lysates were fractionated by SDS-PAGE and transferred to PVDF membranes (BioRad). Blots were blocked in 8% BSA/TBST for 1 h at room temperature and then incubated overnight at 4°C with

1:1000 anti-phospho-VEGFR-2-Y996 antibody (specifically detects phosphorylated tyrosine-996 on VEGFR-2; Cell Signaling) in 4% BSA/TBST. Blots were washed with TBST, incubated with secondary antibody (1:1000 HRP-conjugated goat anti-rabbit IgG) in 5% milk/TBST, washed, detected with enhanced chemiluminescent reagents (Amersham), and exposed to film. Autoradiographs were quantified by scanning on a FluorS imager (BioRad) and data normalized to untreated controls. To confirm equal loading of protein, blots were stripped in SDS/Tris at 50 °C, followed by immunoblot analysis in 1:1000 anti-VEGFR-2 antibody in 5% milk/TBST. The results are shown in Table 3.

These cell-based phosphorylation studies were conducted on ice to reduce VEGFR-2 receptor internalization. Cold temperatures are commonly used in studies of receptor internalization to prevent receptor turnover that may interfere with data interpretation. Moreover, while this assay format was used for the primary screening of compounds, follow-up experiments were performed in these cells at 37 °C for lead compounds and confirmed the observations that were reported at 4 °C.

In Vivo Studies. Inhibitor **61** was evaluated in vivo using standard pharmacological test procedures, which measures the ability to inhibit the growth of human tumor xenografts. Human colon carcinoma DLD-1 cells (American Type Culture Collection, Manassas, VA) were grown in tissue culture in DMEM (Gibco/BRL, Gaithersburg, MD) supplemented with 10% FBS (Gemini Bio-Products Inc., Calabasas, CA). Athymic *nu/nu* female mice (Charles River, Wilmington, MA) were injected subcutaneously (sc) in the flank area with 6×10^6 DLD-1 cells. When tumors attained a mass of between 120 and 160 mg, the mice were randomly assigned into treatment groups containing 5–10 animals per group. Animals were treated either orally (po) once daily with 100 mg/kg **61** prepared in 0.5% Methocel/0.4% Tween 80 or vehicle alone on days 1–20 poststaging (day zero) or intraperitoneal (ip) on days 1, 5, 9, and 13 with 100 or 200 μ g per dose bevacizumab prepared in 0.9% saline. Tumor mass was determined every 7 days [(length \times width²)/2] for 21 days poststaging. Relative tumor growth (mean tumor mass on days 7, 14, and 21 divided by the mean tumor mass on day zero) was determined for each treatment group. Statistical analysis (one-tailed Student's *t*-test) of log relative tumor growth was used to compare the treated versus control group in each experiment. A *p*-value ≤ 0.05 indicates a statistically significant reduction in relative tumor growth of treated group compared to the vehicle control.

Kinetic Experiments. Determinations of the Half-Life ($t_{1/2}$) of Inhibitors in the Presence of Glutathione. Solutions containing 1 μ M or 10 μ M of the inhibitor, 10 μ M of an internal standard, and 100 μ M of reduced glutathione in CH₃CN–H₂O (1:1) were prepared. The reaction mixtures were maintained at ambient temperature without protection from air. The amount of inhibitor remaining as a function of time was monitored using an Agilent LC-1100-MSD equipped with a Phenomenex Luna C5 5 μ m column (50 \times 4.6 mm). Injection volumes were 5 μ L. The mobile phase flow rate was 1.0 mL/min. The HPLC mobile phase gradient was optimized for each compound. For a typical example, the separation was initiated at 25% eluent B, followed by a linear increase to 95% eluent B over 15 min. Eluent A was 10 mM ammonium acetate in 95% water–5% CH₃CN, and eluent B was 10 mM ammonium acetate in 5% water 95% CH₃CN. The HPLC column temperature was maintained at 40 °C during the experiment. Detection was conducted by single-ion-monitoring (SIM) of electrosprayed positive ions of the drug and internal standard. From the rate plot of the data and assuming pseudo-first-order reaction kinetics, the $t_{1/2}$ was determined from the equation $t_{1/2} = \ln(2)/k$, where *k* is the exponential rate of decay.

Matrix-Assisted Laser Desorption/Ionization Mass Spectrometry (MALDI-MS). The MALDI experiments were performed using an Applied Biosystems Voyager Elite STR MALDI mass spectrometry system equipped with a nitrogen laser and delayed extraction. About 0.25–0.6 μ L of the reaction products was mixed with 1 μ L of freshly prepared saturated

sinapinic acid matrix in 0.1% TFA (70:30 H₂O:CH₃CN), spotted on the MALDI plate, slowly dried, and then analyzed.

HPLC Electrospray Ionization Mass Spectrometry (HPLC–ESI-MS). Electrospray ionization mass spectra were obtained in the positive ionization mode with a Waters-Micromass LCT electrospray time-of-flight mass spectrometer. The samples were analyzed with a capillary voltage of 3500 V and cone voltage of 30 V. N₂ was used as the nebulizer and desolvation gas with flow rates of 275 and 675 L/h, respectively. The desolvation temperature was set to 180 °C and the source temperature to 120 °C. The appropriate scans were averaged, smoothed, baseline subtracted, and for protein data transformed using the Micromass transform or maximum entropy programs. The solvent gradients used were CH₃CN:H₂O from 5:95 to 95:5 (v/v) containing 0.2% formic acid. For protein–drug reaction assays, a Waters Symmetry 300 C4 column was used (1 \times 150 mm, 5 μ m particles, Cat # 186000276) with a solvent flow rate of 50 μ L/min for 1 h. For protein digest assays, a Waters Symmetry 300 C18 column was used (1 \times 150 mm, 5 μ m particles, Cat # 186000185) with a solvent flow rate of 65 μ L/min for 90 min. Exact mass measurements were achieved by use of buffer ions and trypsin fragment ions found within the retention time window of the unknown as internal reference ions.

Protein–Drug Reactions for Mass Spectrometry. Samples of VEGFR-2, BSA, and HSA (3–5 μ M) were each incubated with the inhibitors at a molar ratio of 1:10 at 25 °C. The reaction products were sampled after 1 h for the MALDI-MS experiments. For the ESI-MS kinetics experiment, VEGFR-2 samples were analyzed at 0, 2.5, 5, and 20 h incubation times.

Trypsin Proteolysis Reactions for Mass Spectrometry. Sequencing grade trypsin was purchased from Promega (Madison, WI, Cat # V511A) and used to cleave the peptide bonds C-terminally at lysine and arginine residues. For the VEGFR-2 control, 20 μ L of VEGFR-2 (3.8 μ M, prepared at pH of 7.5 in 25 mM HEPES, 75 mM NaCl and 30% glycerol) was incubated with 1.25 μ L of 0.1 μ g/ μ L trypsin and 2 μ L DMSO and the mixture incubated overnight at 25 °C. The molar ratio of VEGFR-2 to trypsin was 15:1. For the reaction of VEGFR-2 with **16**, 50 μ L of VEGFR-2 was mixed with 1.5 μ L of 2.28 mM of **16** (in DMSO) and 3.5 μ L DMSO, which reacted overnight at 25 °C. The molar ratio of VEGFR-2 to **16** was 1:10. To remove the excess drug, the reaction products were washed four times with ~ 100 μ L of 4 mM HEPES solution (pH 8) using a Microcon ultrafiltration filter with a 10 kDa cutoff membrane (Cat. # YM-10). The filtrate was discarded, and the retentate was treated with 3 μ L of 0.1 μ g/ μ L trypsin, incubated overnight at 25 °C, and then analyzed by HPLC–ESI-MS.

Molecular Modeling. The inhibitor structures were minimized using the MMFF94 force field in Sybyl⁴³ and conformationally expanded using Omega⁴⁴ with a 1.0 Å rmsd cutoff to filter out degenerate conformers. A public domain crystal structure of VEGFR-2²⁵ was used as the 3-D representation for molecular docking studies. FRED³⁷ was used for the docking studies. Briefly, FRED uses a shape-based matching of all possible orientations of each conformer and optimizes in accordance with the selected scoring function. The PLP, or piece-wise linear potential function, was used to score the poses docked using FRED, consisting of a steric matching function with a less stringent charge matching function of protein–ligand interactions. The top 10 poses obtained from the FRED docking procedure were rescored with a Poisson Boltzmann molecular mechanics scoring function (PBMM-SA),³⁸ where the free energy of protein–ligand binding is described as

$$\Delta G_{\text{bind}}^{\text{solv}} = \Delta G_{\text{bind}}^{\text{gas}} - \Delta G_{\text{solv}}^{\text{P}} - \Delta G_{\text{solv}}^{\text{L}} + \Delta G_{\text{solv}}^{\text{PL}}$$

where the first term to the right of the equal sign is the gas-phase protein–ligand binding energy and is obtained via molecular mechanics calculations. The remainder of the terms represent the solvated free energy terms for the protein and ligand individually as well as the protein–ligand complex. The

solvated free energy terms are evaluated explicitly via Poisson Boltzmann/surface area calculations. Solvation and hydrophobic effects are aptly handled by this scoring function, which is used to rescore or fine-tune the docked views.

Semiempirical Molecular Orbital Calculations. Inhibitor structures optimized as described above were put into a Sybyl database. It should be noted that the structures were inspected to determine the quinazoline–NH–quinone rotomer. In accordance with the binding mode determined from the structure-based molecular modeling studies, rotomers that favor intramolecular interactions between the quinone carbonyl and the linker NH were chosen. Using the MMFF94 force field within Sybyl, a Powell minimization carried out to an energy gradient of 0.005 kcal/mol Å was performed on each structure in the database. The orbital energies of the lowest unoccupied molecular orbitals (LUMO) were computed for all of the quinones that were prepared using the MOPAC software package interfaced through Sybyl under the AM1 paradigm. No geometry optimization was done at this stage. For a select set of 13 inhibitors (Table 2), the conformational dependence of molecular orbital calculations was evaluated. Using the Sybyl software package, a systematic grid search of the dihedral angles pertaining to the quinazoline–NH–quinone and those on the quinone substituents was carried out at 30° and/or 60° intervals with Powell energy minimization using the MMFF94 force field (energy gradient ≤ 0.005 kcal/mol Å) at each step of the grid search. The set of resulting conformers and energies was imported into a spreadsheet and sorted in order of ascending energies, and Boltzmann averaging of the computed LUMO energies was carried out.⁴⁵ The Boltzmann weight, W_i , for each of the N conformers was computed as follows:

$$W_i = \frac{e^{-(E_i - E_0)/KT}}{\sum_{i=1}^N e^{-(E_i - E_0)/KT}}$$

The computed LUMO energy for each conformation, L_i , was then weighted and summed over all N conformers to give the Boltzmann averaged LUMO energy as follows:

$$\langle \text{LUMO} \rangle = \sum_{i=1}^N W_i L_i$$

Chemistry. ¹H NMR spectra were determined with a Bruker DRX400 spectrometer at 400 MHz. Chemical shifts, δ , are in parts per million relative to the internal standard tetramethylsilane. Electrospray (ES) mass spectra were recorded in positive mode on a Micromass platform spectrometer. Electron impact (EI) and high-resolution mass spectra (HRMS) were obtained on a Finnigan MAT-90 spectrometer. Some high-resolution electrospray mass spectra with higher precision were obtained on a Bruker 9.4T FTMS spectrometer. Chromatographic purifications were by flash chromatography using Baker 40 μ m silica gel. Melting points were determined in open capillary tubes on a Meltemp melting point apparatus and are uncorrected. Analytical HPLC was conducted on an HP 1090 liquid chromatography system over a 4.6 mm \times 150 mm YMC ODS-A column (5 μ m, 120 Å) using multiple wavelength UV detection (typically 230 and 254 nm). For system A, a gradient elution of increasing concentrations of CH₃CN in H₂O containing 0.02% TFA (30–90% over 20 min, wavelength 230 nm) and a flow rate of 1 mL/min was employed. For system B, a gradient elution of increasing concentrations of methanol in H₂O containing 0.02% TFA (70–90% over 20 min, wavelength 230 nm) and a flow rate of 1 mL/min was employed. For system C, a gradient elution of increasing concentrations of CH₃CN in H₂O containing 0.02% TFA (40–90% over 20 min, wavelength 254 nm) and a flow rate of 1 mL/min was employed. For system D, a gradient elution of increasing concentrations of methanol in H₂O containing 0.02% TFA (70–90% over 20 min, wavelength 254

nm) and a flow rate of 1 mL/min was employed. For system E, a gradient elution of increasing concentrations of CH₃CN in H₂O containing 0.02% TFA (40–90% over 20 min, wavelength 230 nm) and a flow rate of 1 mL/min was employed. For system F, a gradient elution of increasing concentrations of CH₃CN in H₂O containing 0.02% TFA (10–90% over 20 min, wavelength 254 nm) and a flow rate of 1 mL/min was employed. For system G, a gradient elution of increasing concentrations of CH₃CN in H₂O containing 0.02% TFA (20–60% over 20 min, wavelength 230 nm) and a flow rate of 1 mL/min was employed. Preparative HPLC was conducted on a Gilson reverse phase HPLC system over a 30 mm \times 150 mm Luna C₁₈ (2) column (10 μ m, 100 Å) using UV wavelength detection at 254 or 215 nm. A gradient elution of increasing concentrations of CH₃CN in H₂O containing 0.02% TFA (20–80% over 20 min) and a flow rate of 40 mL/min was employed.

3-Methoxy-4-(2-methoxyethoxy)benzotriazole (3). A solution of 4-cyano-2-methoxyphenol (522 g, 3.50 mol) in anhydrous DMF (2.0 L) was stirred and cooled with a H₂O bath. K₂CO₃ (725 g, 5.25 mol) was added in portions and the mixture was stirred at 20 °C for 1 h. Bromoethyl methyl ether (427.5 mL, 632.3 g, 4.55 mol) was added dropwise over 1 h. The resulting mixture was stirred at room temperature overnight and then heated at 34–40 °C for 6 h. TLC showed no more starting material remaining. The mixture was poured into a mixture of ice/H₂O (5 kg) and the product precipitated. After stirring for 10 min, the mixture was filtered. The solid was washed with H₂O (3 \times 1.5 L) and air-dried to give **3** (690.0 g, 95%) as a beige solid: MS (ESI, m/z) 208.1 (M + H)⁺; ¹H NMR (400 MHz, CDCl₃) δ 3.45 (s, 3 H), 3.75–3.84 (m, 2 H), 3.88 (s, 3 H), 4.09–4.29 (m, 2 H), 6.93 (d, J = 8.31 Hz, 1 H), 7.08 (d, J = 1.76 Hz, 1 H). Anal. (C₁₁H₁₃NO₃) C, H, N.

5-Methoxy-4-(2-methoxyethoxy)-2-nitrobenzotriazole (4). To a stirred solution of **3** (16.7 g, 80.6 μ mol) in 100 mL of trifluoroacetic anhydride and 70 mL of chloroform was added solid ammonium nitrate (9.7 g, 120.9 μ mol) portionwise over 10 min. The mixture warmed to a gentle boil during the addition. After 2 h, the mixture was diluted with hexanes and the solid was collected. The solid was washed with hexanes, H₂O, dilute NaHCO₃ solution, and then H₂O again. This solid was air-dried to yield 18.4 g of **4** as a light yellow solid: MS (ESI, m/z) 251.97 (M + H)⁺; ¹H NMR (400 MHz, DMSO-*d*₆) δ 3.20–3.39 (s, 3 H), 3.58–3.78 (m, 2 H), 3.98 (s, 3 H), 4.24–4.43 (m, 2 H), 7.70 (s, 1 H), 7.91 (s, 1 H). Anal. (C₁₁H₁₂N₂O₅) C, H, N.

2-Amino-5-methoxy-4-(2-methoxyethoxy)benzotriazole (5). A mixture of **4** (717 g, 2.84 mol) and Pd/C (10%, 45 g) in anhydrous ethanol (6 L) was stirred and heated under reflux. Cyclohexene (1440 mL, 1168 g, 14.2 mol) was added dropwise over 3.5 h. The mixture was refluxed overnight until no more starting material was present by TLC. The mixture was cooled to 40 °C, filtered through a Magnesol pad, and washed with ethanol (4 \times 500 mL). The filtrate was concentrated to give a solid. The solid was collected by filtration, washed with ethanol (2 \times 500 mL), and dried under nitrogen to give a crude product (520 g, 93.7% pure on HPLC). The crude product was suspended in ethanol (750 mL), stirred at 40 °C for 30 min, cooled to room temperature, filtered, washed with ethanol (300 mL), and dried under nitrogen to produce pure **5** (498.2 g, 79%, 97.5% on HPLC) as a yellow solid: mp 102–103 °C; MS (ESI, m/z) 223.15 (M + H)⁺; ¹H NMR (400 MHz, DMSO-*d*₆) δ 3.20–3.41 (m, 3 H), 3.57–3.73 (m, 5 H), 3.92–4.14 (m, 2 H), 5.59 (s, 2 H), 6.33–6.47 (m, 1 H), 6.83–6.95 (m, 1 H).

N'-[2-Cyano-4-methoxy-5-(2-methoxyethoxy)phenyl]-N,N-dimethylformamide (6). A suspension of **5** (495.4 g, 2.229 mol) in DMF–DMA (1.1 L, 8.28 mol) was stirred, heated under reflux for 7 h, and cooled to room temperature. The solid was collected, washed with ether (2 \times 500 mL), and dried under nitrogen at room temperature to give **6** (593.1 g, 96%) as a yellow solid: mp 149–150 °C; MS (ESI, m/z) 278.16 (M + H)⁺; ¹H NMR (400 MHz, CDCl₃) δ 3.06 (s, 6 H), 3.44 (s, 3 H), 3.76–3.81 (m, 2 H), 3.82 (s, 3 H), 4.14–4.22 (m, 2 H), 6.50 (s, 1 H), 6.93 (s, 1 H), 7.55 (s, 1 H).

N-(4-Chloro-2,5-dimethoxyphenyl)-6-methoxy-7-(2-methoxyethoxy)quinazolin-4-amine (8a). A solution of **6** (54.8 g, 0.198 mol) and **7a** (40.78 g, 0.218 mol) in AcOH (246 mL) was heated to 110 °C for 1 h. The reaction was cooled to room temperature and diluted with ether. The resulting solid was collected by filtration to give 82 g (99%) of **8a**: mp 214–217 °C; MS (ESI) *m/z* 420.1 (M + H)⁺; ¹H NMR (400 MHz, CDCl₃) δ 3.49 (s, 3 H), 3.84–3.92 (m, 2 H), 3.95 (s, 3 H), 3.97 (s, 3 H), 4.04 (s, 3 H), 4.23–4.37 (m, 2 H), 6.98 (s, 1 H), 7.02 (s, 1 H), 7.27 (s, 1 H), 7.88 (s, 1 H), 8.71 (d, *J* = 4.03 Hz, 2 H).

2-Chloro-5-{[6-methoxy-7-(2-methoxyethoxy)quinazolin-4-yl]amino}benzo-1,4-quinone (9a). Compound **8a** (8.57 g, 20.4 mmol) was dissolved in a hot CHCl₃ (100 mL), diluted with CH₃CN (256 mL) and H₂O (38 mL), and heated to boiling. While still hot the solution was treated with Ce(NH₄)₂(NO₃)₄ (CAN) (27.9 g, 51.0 mmol) in portions over 20 min. The reaction was then stirred for 1 h, diluted with H₂O (300 mL), and extracted with CHCl₃ (5 × 800 mL). The organic solution was dried (MgSO₄) and filtered through a pad of Magnesol (eluted with 10% CH₃OH in EtOAc). The solvent was removed at reduced pressure. The resulting solid was dissolved in boiling CH₃CN (200 mL) and diluted with ether (200 mL). A red solid formed upon cooling and was collected by filtration (5.49 g, 69%): mp 224–226 °C; MS (ESI) *m/z* 390.1 (M + H)⁺; ¹H NMR (400 MHz, CDCl₃) δ 3.49 (s, 3 H), 3.81–3.97 (m, 2 H), 4.07 (s, 3 H), 4.26–4.41 (m, 2 H), 7.03 (s, 1 H), 7.10 (s, 1 H), 7.33 (s, 1 H), 8.29 (s, 1 H), 8.49 (s, 1 H), 8.83 (s, 1 H). Anal. (C₁₈H₁₆-ClN₃O₅) C, H, N.

3-Chloro-2-methoxy-5-{[6-methoxy-7-(2-methoxyethoxy)quinazolin-4-yl]amino}benzo-1,4-quinone (9c). A solution of **9b** (479 mg, 1.13 mmol) in 60 mL of CH₂Cl₂ was stirred as a solution of NaOPh(3H₂O) (211.49 mg, 1.24 mmol) in 40 mL of CH₃OH was added. The reaction was stirred at room temperature for 1.5 h. It was diluted with CH₂Cl₂ and washed with dilute K₂CO₃. The organic layer was separated and dried over MgSO₄. The solvent was removed in vacuo. The residue was chromatographed on Magnesol, eluting with CHCl₃–CH₃OH mixtures. The solvent was removed. The residue was boiled in CH₃CN and cooled. The resulting solid was collected to yield 170 mg (35.8%) of **9c** as a dark red crystalline solid: MS (ESI) *m/z* 420.1 (M + H)⁺; ¹H NMR (400 MHz, CDCl₃) δ 3.49 (s, 3 H), 3.88–3.90 (m, 2 H), 4.06 (s, 3 H), 4.33–4.34 (m, 2 H), 4.39 (s, 3 H), 7.05 (s, 1 H), 7.32 (s, 1 H), 7.99 (s, 1 H), 8.75 (s, 1 H), 8.83 (s, 1 H). Anal. (C₁₉H₁₈ClN₃O₆·0.33H₂O) C, H, N.

2-Chloro-3-methoxy-6-{[6-methoxy-7-(2-methoxyethoxy)quinazolin-4-yl]amino}-5-(methylthio)benzo-1,4-quinone (9d). CH₃SH was bubbled into 50 mL of CH₂Cl₂ for 10 min. Solid **9c** (500 mg, 1.19 mmol) was added and the reaction mixture was stirred at room temperature for 1.5 h. The solvent was removed in vacuo. The residue was dissolved in 50 mL of hot CH₃CN. DDQ (297.4 mg, 1.31 mmol) was added while the solution was still hot. The reaction mixture was stirred for 10 min and then diluted with 400 mL of CH₂Cl₂. The mixture was washed with dilute K₂CO₃. The organic layer was separated, dried over MgSO₄, and passed through a column of Magnesol. The solvent was removed in vacuo. The residue was chromatographed on silica gel, eluting with CH₂Cl₂, CH₂Cl₂–EtOAc, and CH₂Cl₂–EtOAc–CH₃OH. Solvent was removed from product fractions. The residue was treated with ether. The resulting solid was collected and washed with ether to yield 356 mg (64.2%) of **9d** as a blue-black powder: MS (ESI) *m/z* 466.1 (M + H)⁺; MS (ESI) *m/z* 931.1 (2M + H)⁺; HRMS (ESI–FTMS (M + H)⁺ calcd for C₂₀H₂₀ClN₃O₆S 466.08341, found 466.08433; the purity of **9d** was evaluated by two HPLC systems and found to be 100% (system C, *t*_R = 2.74 min) and 96% (system D, *t*_R = 8.63 min); ¹H NMR (400 MHz, CDCl₃) δ 2.32 (s, 3 H), 3.48 (s, 3 H), 3.88–3.90 (m, 2 H), 4.04 (s, 3 H), 4.32–4.35 (m, 5 H), 7.13 (s, 1 H), 7.32 (s, 1 H), 8.01 (bs, 1 H), 8.74 (s, 1 H).

2-Chloro-5-methoxy-3-{[6-methoxy-7-(2-methoxyethoxy)quinazolin-4-yl]amino}benzo-1,4-quinone (9i). A solution of **9h** (2.0 g, 5.19 mmol) was prepared by heating in 50 mL of CHCl₃. A solution of 25 mL of CHCl₃ saturated with HCl was

added. The suspension was stirred at room temperature overnight. The solvent was removed to give a yellow brown solid, which was dissolved in 50 mL of CH₃CN and 10 mL of H₂O. DDQ (1.19 g, 5.24 mmol) was added over 10 min followed by 823 mg (10 mmol) of sodium acetate. The reaction mixture was stirred at room temperature for 1 h, poured into saturated NaHCO₃, and extracted (3×) with CH₂Cl₂. The organic layer was dried over MgSO₄ and concentrated. The residue was purified on a silica gel column, eluting with CH₂Cl₂, EtOAc, and 2-propanol–EtOAc. The solvent was removed from product fractions. The resulting solid was heated in CH₃CN and diluted with ether. After cooling, the solid was collected to yield 1.2 g (57%) of **9i** as a yellow powder: MS (ESI) *m/z* 420 (M + H)⁺; ¹H NMR (400 MHz, DMSO-*d*₆) δ 3.37 (s, 3 H), 3.80–3.82 (m, 2 H), 3.92 (s, 3 H), 4.04 (s, 3 H), 4.38–4.40 (m, 2 H), 6.51 (s, 1 H), 7.38 (s, 1 H), 8.19 (s, 1 H), 8.92 (s, 1 H). Anal. (C₁₉H₁₈-ClN₃O₆) C, H, N. The regiochemistry of **9i** was confirmed by a NOESY NMR experiment.

5-Methoxy-3-{[6-methoxy-7-(2-methoxyethoxy)quinazolin-4-yl]amino}-2-(pyridin-2-ylthio)benzo-1,4-quinone (9j). To a solution of **9h** (359 mg, 0.93 mmol) in 12 mL of CHCl₃ was added 2-mercaptopyridine (113 mg, 1.02 mmol). After 30 min, DDQ (0.21 g, 1.0 mmol) and 6 mL of CH₃CN were added. After stirring for 30 min, the mixture was poured into dilute Na₂CO₃ and extracted with CH₂Cl₂. The solution was dried (MgSO₄) and poured onto a column of Magnesol. The product was eluted with CH₂Cl₂–2-propanol mixtures. Solvent was removed and the residue was recrystallized from CH₃CN–ether to yield 259 mg (56.3%) of **9j** as an orange powder: MS (ESI) *m/z* 495 (M + H)⁺, 248 (M + 2H)²⁺; ¹H NMR (400 MHz, CDCl₃) δ 3.48 (s, 3 H), 3.89–3.90 (m, 5 H), 4.00 (s, 3 H), 4.31–4.33 (m, 2 H), 6.08 (s, 1 H), 7.01 (dd, *J* = 6.55, 5.04 Hz, 1 H), 7.07 (bs, 1 H), 7.20–7.24 (m, 1 H), 7.30–7.33 (m, 1 H), 7.47–7.52 (m, 1 H), 8.33–8.40 (m, 2 H), 8.69 (bs, 1 H). Anal. (C₂₄H₂₂N₄O₆S) C, H, N.

N-[2,5-Dimethoxy-4-(methylthio)phenyl]-6-methoxy-7-(2-methoxyethoxy)quinazolin-4-amine (8l). Compounds **6** (885 mg, 3.19 mmol) and **7l**⁴⁶ (700 mg, 3.51 mmol) were heated to 110 °C in AcOH (4 mL) for 3 h. The reaction was partitioned in H₂O–EtOAc. The solid precipitates were collected and washed with H₂O and EtOAc. The product was purified on a silica gel column, eluting with 2.5% CH₃OH–CH₂Cl₂ to yield 485 mg (35%) of **8l** as a pink solid: MS (ESI) *m/z* 432.1 (M + H)⁺; HRMS (ESI–FTMS (M + H)⁺ calcd for C₂₁H₂₅N₃O₅S 432.15877, found 432.15853; ¹H NMR (400 MHz, CDCl₃) δ 2.44–2.47 (m, 3 H), 3.47–3.50 (m, 3 H), 3.84–3.92 (m, 2 H), 3.97 (s, 6 H), 4.01–4.10 (m, 3 H), 4.28–4.38 (m, 2 H), 6.93 (s, 1 H), 7.03 (s, 1 H), 7.28–7.32 (m, 1 H), 8.55 (s, 1 H), 8.71 (s, 1 H).

2-(Dimethylamino)-5-{[6-methoxy-7-(2-methoxyethoxy)quinazolin-4-yl]amino}benzo-1,4-quinone (10) (Method A). A mixture of 974 mg (2.5 mmol) of **9a** and 5 mL (10 mmol) of dimethylamine solution (2 M in THF) was added to 289 mg (2.5 mmol) of pyridine hydrochloride in 15 mL of THF. The reaction was stirred at room temperature for 3 h. The resulting solid was filtered, washed with H₂O, and dried to give 936 mg (94%) of **10** as a light brown solid: mp 221–224 °C; MS (ESI) *m/z* 399.2 (M + H)⁺; HRMS (ESI–FTMS, (M + H)⁺ calcd for C₂₀H₂₂N₄O₅ 399.16630, found 399.16664; ¹H NMR (400 MHz, CDCl₃) δ 1.57 (s, 3 H), 3.30 (s, 3 H), 3.48 (s, 3 H), 3.80–3.95 (m, 2 H), 4.06 (s, 3 H), 4.30–4.37 (m, 2 H), 5.63 (s, 1 H), 7.13 (s, 1 H), 7.31 (s, 1 H), 7.79 (s, 1 H), 8.82 (s, 1 H), 9.15 (s, 1 H). Anal. (C₂₀H₂₂N₄O₅) C, H, N.

2-{[6-Methoxy-7-(2-methoxyethoxy)quinazolin-4-yl]amino}-5-morpholin-4-ylbenzo-1,4-quinone (11) (Method B). To the solution of 1.13 g (2.5 mmol) of **9a** in 30 mL of THF was added 1 mL (11.5 mmol) of morpholine. The reaction was stirred at room temperature for 3 h. The resulting solid was filtered, washed with THF and H₂O, and dried to give 1.07 g (97.1%) of **11** as a light red solid: mp 239–243 °C; MS (ESI) *m/z* 441.2 (M + H)⁺; HRMS (ESI–FTMS (M + H)⁺ calcd for C₂₂H₂₄N₄O₆ 441.17686, found 441.17668; the purity of **11** was evaluated by two HPLC systems and found to be 93% (system C, *t*_R = 2.94 min) and 100% (system D, *t*_R = 12.47 min); ¹H

NMR (400 MHz, DMSO- d_6) δ 3.06–3.15 (m, 4 H), 3.64 (s, 3 H), 3.68–3.79 (m, 6 H), 4.02 (s, 3 H), 4.27–4.37 (m, 2 H), 7.35 (s, 1 H), 7.46 (s, 1 H), 7.64 (s, 1 H), 8.65–8.78 (bs, 1 H), 8.79 (s, 1 H), 9.27 (s, 1 H).

2-[[6-Methoxy-7-(2-methoxyethoxy)quinazolin-4-yl]amino]-5-phenoxybenzo-1,4-quinone (13) (Method D). To a solution of 1.13 g (2.5 mmol) of **9a** in 25 mL of acetone were added 1.0 g (10.51 mmol) of phenol and 1 g (7.17 mmol) of potassium carbonate. The reaction was stirred at room temperature overnight. The resulting solid was filtered, washed with H₂O, and dried to give 1.058 g (91.7%) of **13** as a dark pink solid: mp 177–180 °C; MS (ESI) m/z 448.2 (M + H)⁺; ¹H NMR (400 MHz, DMSO- d_6) δ 3.34 (s, 3 H), 3.73–3.77 (m, 2 H), 3.99 (s, 3 H), 4.28–4.35 (m, 2 H), 5.60 (s, 1 H), 7.29–7.34 (m, 3 H), 7.39 (t, J = 7.43 Hz, 1 H), 7.48 (s, 1 H), 7.56 (t, J = 7.93 Hz, 2 H), 7.82 (s, 1 H), 8.78–8.80 (s, 1 H), 9.16 (s, 1 H). Anal. (C₂₄H₂₁N₃O₆·0.50H₂O) C, H, N.

2-(2-Methoxyethoxy)-5-[[6-methoxy-7-(2-methoxyethoxy)quinazolin-4-yl]amino]benzo-1,4-quinone (14) (Method C). To the solution of 0.75 g (1.68 mmol) of **13** in 20 mL of CH₂Cl₂ were added 20 mL (253.6 mmol) of 2-methoxyethanol and 5 drops of Et₃N. The reaction was stirred at room temperature overnight. The resulting solid was filtered and washed with ether to give 0.434 g (60.3%) of **14** as a brown solid: mp 211–212 °C; MS (ESI) m/z 430.3 (M + H)⁺; ¹H NMR (400 MHz, CDCl₃) δ 3.45 (s, 3 H), 3.49 (s, 3 H), 3.84 (m, 2 H), 3.89 (m, 2 H), 4.07 (s, 3 H), 4.17 (m, 2 H), 4.34 (m, 2 H), 6.02 (s, 1 H), 7.06 (s, 1 H), 7.32 (s, 1 H), 8.06 (s, 1 H), 8.73 (s, 1 H), 8.81 (s, 1 H). Anal. (C₂₁H₂₃N₃O₇·0.5H₂O) C, H, N.

2-Methoxy-5-[[6-methoxy-7-(2-methoxyethoxy)quinazolin-4-yl]amino]benzo-1,4-quinone (16). A mixture of **9a** (4.55 g, 11.7 mmol), CH₃OH (3.74 g, 11.7 mmol), and Et₃N (3.45 g, 35.1 mmol) in 300 mL of CH₂Cl₂ was refluxed for 3 h. The reaction was cooled and diluted with H₂O. The organic layer was separated and washed with saturated NaHCO₃ solution. The organic solution was passed through a Magnesol plug, eluting with CH₃OH–CH₂Cl₂ mixtures. The solvent was evaporated to yield 1.75 mg (39%) of **16**: mp 245–248 °C; MS (ESI) m/z 386.3 (M + H)⁺; ¹H NMR (400 MHz, CDCl₃) δ 3.49 (s, 3 H), 3.89 (m, 2 H), 3.92 (s, 3 H), 4.08 (s, 3 H), 4.34 (m, 2 H), 5.99 (s, 1 H), 7.07 (s, 1 H), 7.33 (s, 1 H), 8.07 (s, 1 H), 8.76 (s, 1 H), 8.82 (s, 1 H). Anal. (C₁₉H₁₉N₃O₆) C, H, N.

2-[4-(1H-imidazol-1-yl)phenoxy]-5-[[6-methoxy-7-(2-methoxyethoxy)quinazolin-4-yl]amino]benzo-1,4-quinone (18) (Method F). To a mixture of 4-imidazol-1-ylphenol (24.32 mg, 0.152 mmol), 1 N NaOH (116 μ L, 0.116 mmol), and a trace of the phase transfer catalyst Aliquat-336 (tricaprylmethylammonium chloride) in 2 mL of CH₂Cl₂ and 1 mL of H₂O was added **9a** (39.29 mg, 0.101 mmol). More CH₂Cl₂ was added to dissolve the solids. The reaction was shaken at room temperature overnight. The phases were separated. The organic layers were evaporated and purified by ether–CH₃CN recrystallization to yield 36 mg (69%) of **18** as a light brown solid: mp 124–132 °C; MS (ESI) m/z 514.1 (M + H)⁺, 257.7 (M + 2H)²⁺; ¹H NMR (400 MHz, CDCl₃) δ 3.45–3.51 (s, 3 H), 3.85–3.92 (m, 2 H), 4.03–4.10 (s, 3 H), 4.29–4.38 (m, 2 H), 5.81 (s, 1 H), 7.03 (s, 1 H), 7.26 (s, 1 H), 7.29–7.34 (m, 4 H), 7.50–7.55 (m, 2 H), 7.89 (s, 1 H), 8.18 (s, 1 H), 8.66 (s, 1 H), 8.84 (s, 1 H). Anal. (C₂₇H₂₃N₅O₆·1.25 H₂O) C, H, N.

2-[2-Fluoro-1-(fluoromethyl)ethoxy]-5-[[6-methoxy-7-(2-methoxyethoxy)quinazolin-4-yl]amino]benzo-1,4-quinone (26) (Method E). A mixture of **9a** (60 mg, 0.15 mmol), 1,3-difluoro-2-propanol (147.84 mg, 1.54 mmol), and NaOPh(3H₂O) (51 mg, 0.3 mmol) in 2 mL of CH₂Cl₂ was shaken at room temperature overnight. The reaction was diluted with H₂O, and the layers were separated. The organic layer was washed three times with saturated K₂CO₃ and was passed through a plug of Magnesol, eluting with CH₂Cl₂ followed by 1% CH₃OH–CH₂Cl₂. The solvent was removed in vacuo to yield 18 mg (26.7%) of **26**: MS (ESI) m/z 450.2 (M + H)⁺; HRMS (ESI–FTMS (M + H)⁺) calcd for C₂₁H₂₁F₂N₃O₆ 450.14712, found 450.14647; ¹H NMR (400 MHz, CDCl₃) δ 3.49 (s, 3 H), 3.89 (m, 2 H), 4.07 (s, 3 H), 4.34 (m, 2 H), 4.61–4.73 (m, 2 H), 4.75–4.91 (m, 3 H), 6.13 (s, 1 H), 7.04 (s, 1 H), 7.32

(s, 1 H), 8.08 (s, 1 H), 8.67 (s, 1 H), 8.82 (s, 1 H). Anal. (C₂₁H₂₁F₂N₃O₆·0.33 H₂O) C, N, H: calcd, 4.38; found, 4.8.

2-[(2-Hydroxypropyl)amino]-5-[[6-methoxy-7-(2-methoxyethoxy)quinazolin-4-yl]amino]benzo-1,4-quinone (41). A solution of **21** (250 mg, 0.64 mmol) in 250 mL of THF and 250 mL of H₂O was adjusted to pH 4 with concentrated HCl and stirred for 18 h. The aqueous solution was extracted three times with 150 mL of CH₂Cl₂. The CH₂Cl₂ layer was separated, dried over Na₂SO₄, and concentrated. The residue was chromatographed on a short silica gel pad, eluting with 7% 2-propanol–CH₂Cl₂. The solvent of the product fraction was evaporated to give 190 mg (69%) of **41**: MS (ESI) m/z 429.2 (M + H)⁺; HRMS (ESI–FTMS (M + H)⁺) calcd for C₂₁H₂₄N₄O₆ 429.17686, found 429.17515; ¹H NMR (400 MHz, DMSO- d_6) δ 1.10 (d, J = 8 Hz, 3 H), 3.04–3.13 (m, 1 H), 3.14–3.22 (m, 1 H), 3.34 (s, 3 H), 3.72–3.78 (m, 2 H), 3.82–3.93 (m, 1 H), 4.02 (s, 3 H), 4.30–4.34 (m, 2 H), 4.97 (d, J = 5.04 Hz, 1 H), 5.60 (s, 1 H), 7.35–7.41 (m, 2 H), 7.62–7.68 (m, 2 H), 8.81 (s, 1 H), 9.51 (s, 1 H). Anal. (C₂₁H₂₄N₄O₆·0.25H₂O) C, H, N.

2-[[6-Methoxy-7-(2-methoxyethoxy)quinazolin-4-yl]amino]-5-(5-methyl-2-oxo-1,3-oxazolidin-3-yl)benzo-1,4-quinone (42). A mixture of **41** (130 mg, 0.30 mmol) and carbonyldiimidazole (488 mg, 3 mmol) in 10 mL of dry 1-methyl-2-pyrrolidinone was stirred under N₂ for 27 h. The mixture was poured into H₂O and extracted with EtOAc and dried. The solvent was removed and the residue was chromatographed on a silica gel column, eluting with 4% 2-propanol–CH₂Cl₂. The solvent from the product fractions was evaporated to give 55 mg (42%) of **42**: MS (ESI) m/z 455.1 (M + H)⁺; HRMS (ESI–FTMS (M + H)⁺) calcd for C₂₂H₂₂N₄O₇ 455.15613, found 455.15478; ¹H NMR (400 MHz, CDCl₃) δ 1.52 (d, J = 6.04 Hz, 4 H), 3.49 (s, 3 H), 3.87–3.91 (m, 2 H), 4.08 (s, 3 H), 4.32–4.35 (m, 2 H), 4.54 (dd, J = 10.95, 7.93 Hz, 1 H), 4.69–4.79 (m, 1 H), 7.07 (s, 1 H), 7.31–7.33 (s, 1 H), 7.60 (s, 1 H), 8.00 (s, 1 H), 8.68 (s, 1 H), 8.83 (s, 1 H). Anal. (C₂₂H₂₂N₄O₇) C, H, N.

2-Chloro-4-hydroxy-3-methoxy-5-nitrobenzaldehyde (45). To a stirred solution of **43**³¹ (21.33 g, 77.95 mmol) and dimethyl sulfate (90 mL, 0.952 mol) in EtOH (192 mL) at 40 °C was added a 40% solution of KOH (140 mL, 98.2 mol) dropwise over 45 min. The reaction was then stirred at 55 °C for 1 h. The solvent was evaporated and the residue was extracted with ether (2 \times). The ether solution was dried (MgSO₄) and was passed through a column of Magnesol. The solvent was removed to give 22.3 g (90.91 mmol) of **44** as a colorless oil. This was mixed with H₂O (1.12 mL) and LiCl (23.12 g, 0.545 mol) in 123 mL of DMF and heated at 110 °C for 3 h. The dark red mixture was cooled and treated with a solution of saturated NaHCO₃ (59 mL) and H₂O (800 mL). The aqueous solution was washed with ether (2 \times), made acidic with H₂SO₄, and cooled to 4 °C. The resulting solid was collected by vacuum filtration, washed with H₂O, and dried in air to give 18.3 g (87%) of **45** as an off white solid: MS (ESI) m/z 230 (M + H)⁺; ¹H NMR (400 MHz, CDCl₃) δ 4.01 (s, 3 H), 8.54 (s, 1 H), 10.35 (s, 1 H), 11.14 (s, 1 H).

2-Chloro-3-methoxy-5-nitrobenzene-1,4-diol (46). To compound **45** (17.8 g, 72.47 mmol) were added 1 N NaOH (72.5 mL, 72.5 mmol), H₂O (158 mL), 30% H₂O₂ (45 mL), and CH₃OH (158 mL). The mixture was stirred at 50 °C for 3.5 h. The CH₃OH was evaporated and the solution was cooled in an ice bath. The resulting solid was collected by vacuum filtration, washed with H₂O, and air-dried to give 7.9 g (50%) of **46** as an orange solid: MS (ESI) m/z 218 (M + H)⁺; ¹H NMR (400 MHz, CDCl₃) δ 4.01 (s, 3 H), 5.43 (s, 1 H), 7.56 (s, 1 H), 10.37 (d, J = 11.33 Hz, 1 H).

2-Chloro-1,3,4-trimethoxy-5-nitrobenzene (47). Compound **46** (7.8 g, 35.53 mmol) in 77 mL of DMF was stirred with dimethyl sulfate (11.2 g, 88.81 mmol) and K₂CO₃ (14.73 g, 106.57 mmol) at 80 °C for 1 h. The mixture was poured into H₂O and the resulting solid was collected by vacuum filtration, washed with H₂O, and air-dried to give 8.0 g (91%) of **47** as a gray solid: MS (APCI) m/z 247.1; MS (APCI) m/z 247.1; ¹H NMR (400 MHz, CDCl₃) δ 3.96 (t, J = 8.0 Hz, 9 H), 7.17 (s, 1 H).

4-Chloro-2,3,5-trimethoxy-phenylamine (7e). A solution of **47** (8.0 g, 32.31 mmol), Fe (10.83 g, 193.33 mmol), and AcOH (11.1 mL, 193.83 mmol) in CH₃OH (429 mL) was refluxed with mechanical stirring for 2 h. The reaction was then treated with NaOH (10 M, 19.38 mL, 193.83 mmol) and filtered. The solid was washed with EtOAc. The filtrate was concentrated, redissolved in EtOAc, washed with saturated NaHCO₃, dried (MgSO₄), and concentrated to give 6.17 g of **7e** as a light tan oil. This material was used without additional purification.

2,3-Dimethoxy-5-[[6-methoxy-7-(2-methoxyethoxy)-quinazolin-4-yl]amino]benzo-1,4-quinone (49). To a solution of **9e** (800 mg, 1.91 mmol) in CH₂Cl₂ (115 mL) were added CsCO₃ (825 mg, 2.53 mmol) and CH₃OH (57 mL, 1.45 mol). The reaction mixture was stirred at room temperature for 2.5 h and filtered through a short column of silica gel. The solvent evaporated and the residue was chromatographed on silica gel, eluting with CHCl₃-EtOAc from 7:3 to 5:5. Product fractions were collected and concentrated. The residue was stirred in small amount of CH₃CN. The resulting solid was filtered to yield 0.2 g (25%) of **49** as a red crystalline solid: MS (ESI) *m/z* 416.1 (M + H)⁺; ¹H NMR (400 MHz, CDCl₃) δ 3.45–3.50 (s, 3 H), 3.85–3.90 (m, 2 H), 3.98 (s, 3 H), 4.07 (s, 3 H), 4.20 (s, 3 H), 4.30–4.38 (m, 2 H), 7.06 (s, 1 H), 7.32 (s, 1 H), 7.93–7.93 (s, 1 H), 8.66 (s, 1 H), 8.80 (s, 1 H). Anal. (C₂₀H₂₁N₃O₇·0.5H₂O) C, H, N.

2-[2-Fluoro-1-(fluoromethyl)ethoxy]-3-methoxy-5-[[6-methoxy-7-(2-methoxyethoxy)quinazolin-4-yl]amino]benzo-1,4-quinone (50). To a solution of **9e** (650 mg, 1.55 mmol) in CH₂Cl₂ (93 mL) was added CsCO₃ (671 mg, 2.06 mmol) and 1,3-difluoro-2-propanol (4.46 g, 46.45 mmol). The reaction mixture was stirred at room temperature overnight. The mixture was filtered through a short column of silica gel, eluting with CHCl₃/EtOAc = 1:1. The solvent was removed and the residue was stirred with ether. The resulting solid was filtered to yield 0.25 g (33.6%) of **50** as a red solid: MS (ESI) *m/z* 480.1 (M + H)⁺; HRMS (ESI-FTMS (M + H)⁺) calcd for C₂₂H₂₃F₂N₃O₇ 480.15768, found 480.15833; ¹H NMR (400 MHz, CDCl₃) δ 3.45–3.50 (s, 3 H), 3.87–3.91 (m, 2 H), 4.06 (s, 6 H), 4.28–4.39 (m, 2 H), 4.65–4.73 (m, 2 H), 4.78–4.87 (m, 2 H), 5.07–5.22 (m, 1 H), 7.04 (s, 1 H), 7.33 (s, 1 H), 7.91–7.94 (s, 1 H), 8.59 (s, 1 H), 8.82 (s, 1 H). The purity of **50** was evaluated by two HPLC systems and found to be 100% (system C, *t*_R = 3.89 min) and 89% (system D, *t*_R = 12.2 min).

(4-Chloro-2, 5-dimethoxyphenyl)(4-methoxybenzyl)-amine (54). Under N₂, to a stirred solution of the *p*-anisaldehyde **53** (35.4 g, 260 mmol) in CH₂Cl₂ (750 mL) were added **7a** (46.9 g, 250 mmol), sodium triacetoxymethylborohydride (79.5 g, 375 mmol), and acetic acid (21.5 mL, 375 mmol). The reaction mixture was stirred at room temperature for 2.5 h. H₂O was added and the mixture was adjusted to pH 9–10 with K₂CO₃. The CH₂Cl₂ layer was washed with H₂O, dried, and concentrated. The residue was dissolved in 3:1 hexanes-EtOAc (500 mL) and passed through a 8.0 × 4.0 cm pad of silica gel. The solvent was evaporated to yield 77.1 g (96%) of **54** as a white solid: mp 53–63 °C; MS (ESI) *m/z* 308 (M + H)⁺; ¹H NMR (400 MHz, CDCl₃) δ 3.77 (d, *J* = 5.54 Hz, 6 H), 3.80 (s, 3 H), 4.26 (s, 2 H), 4.57 (bs, 1 H), 6.25 (s, 1 H), 6.75 (s, 1 H), 6.84–6.94 (m, 2 H), 7.24–7.34 (m, 2 H).

N-(4-Chloro-2,5-dimethoxyphenyl)-7-fluoro-6-methoxy-N-(4-methoxybenzyl)quinazolin-4-amine (56). A mixture of **54** (30.8 g, 100 mmol), **55**,³³ and pyridine (0.65 mL) in *tert*-butyl alcohol (240 mL) under nitrogen was stirred at reflux temperature for 24 h. The *tert*-butyl alcohol was removed at reduce pressure. The residue was stirred with CH₂Cl₂ and diluted with NH₄OH. The insoluble material was removed by filtration. The CH₂Cl₂ layer was washed with brine, dried over MgSO₄, and evaporated to give 148.4 g of a dark red gum. The gum was dissolved into 40:1 CH₂Cl₂-EtOAc (30 mL) and placed on a silica gel column (3.6 × 4.2 cm), which was eluted with 40:1 CH₂Cl₂-EtOAc to yield 31 g (80%) of **56** as a white solid: mp amorphous; ¹H NMR (400 MHz, DMSO-*d*₆) δ 3.34 (d, *J* = 2.01 Hz, 6 H), 3.70 (d, *J* = 5.29 Hz, 6 H), 5.27 (s, 2 H), 6.63 (d, *J* = 9.57 Hz, 1 H), 6.78–6.86 (m, 2 H), 7.12 (s, 1 H),

7.21 (s, 1 H), 7.26–7.36 (m, 2 H), 7.56 (d, *J* = 12.34 Hz, 1 H), 8.65 (s, 1 H).

N-(4-Chloro-2,5-dimethoxyphenyl)-6-methoxy-7-[(1-methylpiperidin-4-yl)methoxy]quinazolin-4-amine (58a). To a stirred mixture of **56** (2.07 g, 4.27 mmol) and **57a** (1.09 g, 8.6 mmol) in THF (4.0 mL) under nitrogen at 25 °C was added sodium bis(trimethylsilyl)amide (1.0 M in THF, 10.6 mL, 10.6 mmol) over 30 s. The reaction mixture was refluxed for 30 min, cooled, and partitioned between CH₂Cl₂ and H₂O. The CH₂Cl₂ layer was washed with brine, dried over MgSO₄, and evaporated. A solution of the resulting gum in TFA (25 mL) was stirred at 55–60 °C for 45 min and concentrated to dryness. The residue was partitioned between CH₂Cl₂ and aqueous NaHCO₃. The CH₂Cl₂ layer was washed with brine, dried over MgSO₄, and evaporated. The residue was purified on a flash column of silica gel (2 × 20 cm), eluting with 3:1 CH₂Cl₂-EtOAc and 25:25:1 CH₂Cl₂-EtOAc-CH₃OH to yield 1.75 (87%) of **58a** as a solid: MS (ESI) *m/z* 473.2 (M + H)⁺, 237.1 (M + 2H)²⁺; ¹H NMR (400 MHz, DMSO-*d*₆) δ 1.28–1.45 (m, 2 H), 1.76 (d, *J* = 10.07 Hz, 3 H), 1.87 (t, *J* = 10.83 Hz, 2 H), 2.16 (s, 3 H), 2.79 (d, *J* = 11.08 Hz, 2 H), 3.75 (s, 3 H), 3.80 (s, 3 H), 3.93 (s, 3 H), 3.99 (d, *J* = 6.04 Hz, 2 H), 7.15 (s, 1 H), 7.22 (s, 1 H), 7.38 (s, 1 H), 7.79 (s, 1 H), 8.32 (s, 1 H), 9.18 (s, 1 H). Anal. (C₂₄H₂₉ClN₄O₄·0.2CH₄O) C, H, N.

2-((6-Methoxy-7-[(1-methylpiperidin-4-yl)methoxy]quinazolin-4-yl)amino)-5-(2-[methyl(phenyl)amino]ethoxy)benzo-1,4-quinone (62) (Method G). To a solution of 107 mg (0.243 mmol) of **59a** in 3 mL of CH₂Cl₂ was added 158 mg (0.485 mmol) of cesium carbonate and 367 mg (2.43 mmol) of *N*-methyl-2-(phenylamino)ethanol. The reaction was stirred at room temperature for 2 h and 20 min. It was then washed with brine, dried over Na₂SO₄, and concentrated. The product was purified using a Gilson HPLC. The product fractions were neutralized with NaHCO₃ and extracted with CH₂Cl₂. The resulting material was filtered through a plug of Magnesol eluting first with EtOAc (discard) and then with CH₃OH-EtOAc-Et₃N mixtures. The filtrate was concentrated in vacuo to yield 25 mg (18%) of **62**: MS (ESI) *m/z* 558.2 (M + H)⁺, 279.6 (M + 2H)²⁺; HRMS (ESI-FTMS (M + H)⁺) calcd for C₃₁H₃₅N₅O₅ 558.27110, found 558.272; ¹H NMR (400 MHz, CDCl₃) δ 1.88–2.10 (m, 7 H), 2.33 (s, 3 H), 2.90–2.95 (m, 2 H), 3.06–3.11 (s, 3 H), 3.89 (t, *J* = 5.79 Hz, 2 H), 4.02–4.08 (m, 5 H), 4.16 (t, *J* = 5.92 Hz, 2 H), 5.93 (s, 1 H), 6.71–6.81 (m, 3 H), 7.05 (s, 1 H), 7.24–7.30 (m, 3 H), 8.04 (s, 1 H), 8.73 (s, 1 H), 8.80 (s, 1 H). The purity of **62** was evaluated by two HPLC solvent systems and found to be 98% (system G, *t*_R = 2.03 min) and 98% (system B, *t*_R = 2.97 min).

2-[2-Fluoro-1-(fluoromethyl)ethoxy]-5-[[6-methoxy-7-(3-pyrrolidin-1-ylpropoxy)quinazolin-4-yl]amino]benzo-1,4-quinone (65). A solution of **59b** was prepared by CAN oxidation of **58b** (850 mg, 1.8 mmol) and extracting in 500 mL of CHCl₃. To the solution were added 1,3-difluoro-2-propanol (1.39 mL, 18.0 mmol) and NaOPh(3H₂O) (306.2 mg, 1.8 mmol). The reaction mixture was stirred at room temperature for 2 h. The solvent was concentrated to a volume of 80 mL at 40 °C. The reaction mixture was filtered through a plug of Magnesol, eluting with CH₂Cl₂, EtOAc, 25% 2-propanol-EtOAc, and then CH₂Cl₂-EtOAc-2-propanol-Et₃N (200:200:100:6) to yield 97.4 mg (10.7%) of **65** as a red solid: MS (ESI) *m/z* 503.1 (M + H)⁺, 252 (M + 2H)²⁺; HRMS (ESI-FTMS) calcd for C₂₅H₂₈F₂N₄O₅ 503.21005, found 503.21081; ¹H NMR (400 MHz, CDCl₃) δ 1.81 (s, 4 H), 2.08–2.24 (m, 2 H), 2.56 (s, 4 H), 2.69 (t, *J* = 7.18 Hz, 2 H), 4.08 (s, 3 H), 4.28 (t, *J* = 6.55 Hz, 2 H), 4.66–4.72 (m, 2 H), 4.77–4.91 (m, 3 H), 6.13 (s, 1 H), 7.06 (s, 1 H), 7.33 (s, 1 H), 8.10 (s, 1 H), 8.69 (s, 1 H), 8.84 (s, 1 H). The purity of **65** was evaluated by two HPLC systems and found to be 86% (system C, *t*_R = 2.03 min) and 76% (system D, *t*_R = 7.79 min).

Acknowledgment. The authors wish to thank Drs. Tarek Mansour, Philip Frost, Lee Greenberger, and Janis Upešlacis for their support and encouragement. We also would like to thank the members of the Wyeth Discovery Oncology group for in vivo evaluations, and

members of the Wyeth Chemical Technologies group for analytical and spectral determinations.

Supporting Information Available: Additional synthetic procedures and characterization data. This material is available free of charge via the Internet at <http://pubs.acs.org>.

References

- Carmeliet, P.; Jain, R. K. Angiogenesis in cancer and other diseases. *Nature* **2000**, *407*, 249–257.
- Terman, B. I.; Dougher-Vermazen, M.; Carrion, M. E.; Dimitrov, D.; Armellino, D. C.; Gospodarowicz, D.; Bohlen, P. Identification of the KDR tyrosine kinase as a receptor for vascular endothelial cell growth factor. *Biochem. Biophys. Res. Commun.* **1992**, *187*, 1579–1586.
- Folkman, J. Role of angiogenesis in tumor growth and metastasis. *Sem. Oncol.* **2002**, *29*, 15–18.
- Ferrara, N. Vascular endothelial growth factor as a target for anticancer therapy. *Oncologist* **2004**, *9 Suppl 1*, 2–10.
- Hicklin, D. J.; Ellis, L. M. Role of the vascular endothelial growth factor pathway in tumor growth and angiogenesis. *J. Clin. Oncol.* **2005**, *23*, 1011–1027.
- Kerbel, R. S. Inhibition of tumor angiogenesis as a strategy to circumvent acquired resistance to anti-cancer therapeutic agents. *Bioessays* **1991**, *13*, 31–36.
- Browder, T.; Butterfield, C. E.; Kraling, B. M.; Shi, B.; Marshall, B.; O'Reilly, M. S.; Folkman, J. Antiangiogenic scheduling of chemotherapy improves efficacy against experimental drug-resistant cancer. *Can. Res.* **2000**, *60*, 1878–1886.
- Kerbel, R. S.; Kamen, B. A. The anti-angiogenic basis of metronomic chemotherapy. *Nature Rev. Cancer* **2004**, *4*, 423–436.
- Ferrara, N.; Hillan, K. J.; Gerber, H. P.; Novotny, W. Discovery and development of bevacizumab, an anti-VEGF antibody for treating cancer. *Nat. Rev. Drug Dis.* **2004**, *3*, 391–400.
- Sweeney, P.; Karashima, T.; Kim, S. J.; Kedar, D.; Mian, B.; Huang, S.; Baker, C.; Fan, Z.; Hicklin, D. J.; Pettaway, C. A.; Dinney, C. P. Anti-vascular endothelial growth factor receptor 2 antibody reduces tumorigenicity and metastasis in orthotopic prostate cancer xenografts via induction of endothelial cell apoptosis and reduction of endothelial cell matrix metalloproteinase type 9 production. *Clin. Cancer Res.* **2002**, *8*, 2714–2724.
- Pavco, P. A.; Bouhana, K. S.; Gallegos, A. M.; Agrawal, A.; Blanchard, K. S.; Grimm, S. L.; Jensen, K. L.; Andrews, L. E.; Wincott, F. E.; Pitot, P. A.; Tressler, R. J.; Cushman, C.; Reynolds, M. A.; Parry, T. J. Antitumor and antimetastatic activity of ribozymes targeting the messenger RNA of vascular endothelial growth factor receptors. *Clin. Cancer Res.* **2000**, *6*, 2094–2103.
- Tokunaga, T.; Abe, Y.; Tsuchida, T.; Hatanaka, H.; Oshika, Y.; Tomisawa, M.; Yoshimura, M.; Ohnishi, Y.; Kijima, H.; Yamazaki, H.; Ueyama, Y.; Nakamura, M. Ribozyme mediated cleavage of cell-associated isoform of vascular endothelial growth factor inhibits liver metastasis of a pancreatic cancer cell line. *Int. J. Oncol.* **2002**, *21*, 1027–1032.
- Takei, Y.; Kadomatsu, K.; Yuzawa, Y.; Matsuo, S.; Muramatsu, T. A small interfering RNA targeting vascular endothelial growth factor as cancer therapeutics. *Cancer Res.* **2004**, *64*, 3365–3370.
- Underiner, T. L.; Ruggeri, B.; Gingrich, D. E. Development of vascular endothelial growth factor receptor (VEGFR) kinase inhibitors as anti-angiogenic agents in cancer therapy. *Cur. Med. Chem.* **2004**, *11*, 731–745.
- Boyer, S. J. Small molecule inhibitors of KDR (VEGFR-2) kinase: An overview of structure activity relationships. *Curr. Top. Med. Chem.* **2002**, *2*, 973–1000.
- Laird, A. D.; Cherrington, J. M. Small molecule tyrosine kinase inhibitors: Clinical development of anticancer agents. *Exp. Opin. Invest. Drugs* **2003**, *12*, 51–64.
- Steward, W. P.; Thomas, A.; Morgan, B.; Wiedenmann, B.; Bartel, C.; Vanhoefer, U.; Trarbach, T.; Junker, U.; Laurent, D.; Lebowitz, D. Expanded phase III study of PTK787/ZK 22584 (PTK/ZK), a novel, oral angiogenesis inhibitor, in combination with FOLFOLX-4 as first-line treatment for patients with metastatic colorectal cancer. *J. Clin. Oncol.* (2004 ASCO Annual Meeting Proceedings) **2004**, *22*, 3556.
- Raymond, E.; Faivre, S.; Vera, K.; Delbaldo, C.; Robert, C.; Spatz, A.; Bello, C.; Brega, N.; Scigalla, P.; Armand, J. P. Final results of a phase I and pharmacokinetic study of SU11248, a novel multi-target tyrosine kinase inhibitor, in patients with advanced cancers. *Proc. Am. Soc. Clin. Oncol.* **2003**, *22*, 192 (abstr 769).
- Kabbinavar, F.; Hurwitz, H. I.; Fehrenbacher, L.; Meropol, N. J.; Novotny, W. F.; Lieberman, G.; Griffing, S.; Bergsland, E. Phase II, randomized trial comparing bevacizumab plus fluorouracil (FU)/leucovorin (LV) with FU/LV alone in patients with metastatic colorectal cancer [see comment]. *J. Clin. Oncol.* **2003**, *21*, 60–65.
- Johnson, D. H.; Fehrenbacher, L.; Novotny, W. F.; Herbst, R. S.; Nemunaitis, J. J.; Jablons, D. M.; Langer, C. J.; DeVore, R. F., III; Gaudreault, J.; Damico, L. A.; Holmgren, E.; Kabbinavar, F. Randomized phase II trial comparing bevacizumab plus carboplatin and paclitaxel with carboplatin and paclitaxel alone in previously untreated locally advanced or metastatic nonsmall-cell lung cancer. *J. Clin. Oncol.* **2004**, *22*, 2184–2191.
- Torrance, C. J.; Jackson, P. E.; Montgomery, E.; Wissner, A.; Kinzler, K. W.; Vogelstein, B.; Frost, P.; Discifani, C. M. Combinatorial Chemoprevention of Intestinal Neoplasia. *Nat. Med.* **2000**, *6*, 1024–1028.
- Wissner, A.; Overbeek, E.; Reich, M. F.; Floyd, M. B.; Johnson, B. D.; Mamuya, N.; Rosfjord, E. C.; Discifani, C.; Davis, R.; Shi, X.; Rabindran, S. K.; Gruber, B. C.; Ye, F.; Hallett, W. A.; Nilakantan, R.; Shen, R.; Wang, Y.-F.; Greenberger, L. M.; Tsou, H.-R. Synthesis and Structure–Activity Relationships of 6,7-Disubstituted 4-Anilinoquinoline-3-carbonitriles. The Design of an Orally Active, Irreversible Inhibitor of the Tyrosine Kinase Activity of the Epidermal Growth Factor Receptor (EGFR) and the Human Epidermal Growth Factor Receptor-2 (HER-2). *J. Med. Chem.* **2003**, *46*, 49–63.
- Rabindran, S. K.; Discifani, C. M.; Rosfjord, E. C.; Baxter, M.; Floyd, M. B.; Golas, J.; Hallett, W. A.; Johnson, B. D.; Nilakantan, R.; Overbeek, E.; Reich, M. F.; Shen, R.; Shi, X.; Tsou, H.-R.; Wang, Y.-F.; Wissner, A. Antitumor Activity of HKI-272, an Orally Active, Irreversible Inhibitor of the HER-2 Tyrosine Kinase. *Cancer Res.* **2004**, *64*, 3958–3965.
- Tsou, H.-R.; Overbeek, E.; Hallett, W. A.; Reich, M. F.; Floyd, M. B.; Johnson, B. D.; Michalak, R. S.; Nilakantan, R.; Discifani, C.; Golas, J.; Rabindran, S. K.; Shen, R.; Shi, X.; Wang, Y.-F.; Upešlacis, J.; Wissner, A. Optimization of 6,7-Disubstituted-4-(arylamino)quinoline-3-carbonitriles as Orally Active, Irreversible Inhibitors of HER-2 kinase Activity. *J. Med. Chem.* **2005**, *48*, 1107–1131.
- McTigue, M. A.; Wickersham, J. A.; Pinko, C.; Showalter, R. E.; Parast, C. V.; Tempczyk-Russell, A.; Gehring, M. R.; Mroczkowski, B.; Kan, C. C.; Villafranca, J. E.; Appelt, K. Crystal Structure of the Kinase Domain of Human Vascular Endothelial Growth Factor Receptor 2: A Key Enzyme in Angiogenesis. *Struct. Fold Des.* **1999**, *7*, 319–330.
- Hennequin, L. F.; Thomas, A. P.; Johnstone, C.; Stokes, E. S. E.; Plé, P. A.; Lohmann, J.-J. M.; Ogilvie, D. J.; Dukes, M.; Wedge, S. R. Curwen, J. O.; Kendrew, Lambert-van der Brempt, C. Design and Structure–Activity Relationship of a New Class of Potent VEGF Receptor Tyrosine Kinase Inhibitors. *J. Med. Chem.* **1999**, *42*, 5369–5389.
- Wissner, A.; Berger, D. M.; Boschelli, D. H.; Floyd, M. B. Jr.; Greenberger, L. M.; Gruber, B. C.; Johnson, B. D.; Mamuya, N.; Nilakantan, R.; Reich, M. F.; Shen, R.; Tsou, H.-R.; Upešlacis, E.; Wang, Y.-F.; Wu, B.; Ye, F.; Zhang, N. 4-Anilino-6,7-dialkoxyquinoline-3-carbonitrile Inhibitors of Epidermal Growth Factor Receptor (EGFR) Kinase and Their Bioisosteric Relationship to the 4-Anilino-6,7-dialkoxyquinazoline Inhibitors. *J. Med. Chem.* **2000**, *43*, 3244–3256.
- Shewchuk, L.; Hassell, A.; Wisely, B.; Rocque, W.; Holmes, W.; Veal, J.; Kuyper, L. F. Binding Mode of the 4-Anilinoquinazoline Class of Protein Kinase Inhibitor: X-ray Crystallographic Studies of 4-Anilinoquinazolines Bound to Cyclin-Dependent Kinase 2 and p38 Kinase. *J. Med. Chem.* **2000**, *43*, 133–138.
- Stamos, J.; Sliwkowski, M. X.; Eigenbrot, C. Structure of the Epidermal Growth Factor Receptor Kinase Domain Alone and in Complex with a 4-Anilinoquinazoline Inhibitor. *J. Biol. Chem.* **2002**, *277*, 46265–46272.
- Wedge, S. R.; Ogilvie, D. J.; Dukes, M.; Kendrew, J.; Curwen, J. O.; Hennequin, L. F.; Thomas, A. P.; Stokes, E. S. E.; Curry, B.; Richmond, G. H. P.; Wadsworth, P. F. ZD4190: An Orally Active Inhibitor of Vascular Endothelial Growth Factor Signaling with Broad-spectrum Antitumor Efficacy. *Cancer Res.* **2000**, *60*, 970–975.
- Borgulya, J.; Bruderer, H.; Bernauer, K.; Zuercher, G.; Mose, D.-P. Catechol-O-methyltransferase-inhibiting Pyrocatechol Derivatives: Synthesis and Structure–Activity Studies. *Helv. Chim. Acta* **1989**, *72*, 952–968.
- Wissner, A.; Floyd, M. B.; Rabindran, S. K.; Nilakantan, R.; Greenberger, L. M.; Shen, R.; Wang, Y.-F.; Tsou, H.-R. Synthesis and EGFR and HER-2 Kinase Inhibitory Activities of 4-Anilinoquinoline-3-Carbonitriles. Analogues of Three Important 4-Anilinoquinazolines Currently Undergoing Clinical Evaluation as Therapeutic Antitumor Agents. *Bioorg. Med. Chem. Lett.* **2002**, *12*, 2893–2897.
- Barker, A. J.; Brown, D. S. Preparation of Aminoquinazolines Useful in the Treatment of Cancer. Eur. Pat. Appl. EP602851, 1994.
- Magee, P. S. Exploring the Chemistry of Quinones by Computational. *Quant. Struct. Act. Relat.* **2000**, *19*, 22–28.

- (35) Rozeboom, M. D.; Tegmo-Larsson, I.-M.; Houk, K. N. Frontier Molecular Orbital Theory of Substituent Effects on Regioselectivities of Nucleophilic Additions and Cycloadditions to Benzoquinones and Naphthoquinones. *J. Org. Chem.* **1981**, *46*, 2338–2345.
- (36) Takahashi, N.; Schreiber, J.; Fischer, V.; Mason, R. P. Formation of Glutathione-Conjugated Semiquinones by the Reaction of Quinones with Glutathione: An ESR Study. *Arch. Biochem. Biophys.* **1987**, *252*, 41–48.
- (37) *FRED*; Open Eye Scientific Software: Santa Fe, NM (www.eyesopen.com)
- (38) Rush, T. S., III.; Manas, E.; Tawa, G.; and Alvarez, J. Solvation-Based Scoring for High Throughput Docking in Virtual Screening in *Drug Discovery*; Alvarez, J. and Shoichet, B., Eds.; CRC Press: Boca Raton, FL, 2005; pp 241–269.
- (39) Loganzo, F. and Hardy, C. A Sensitive, Time-resolved Fluorometric Assay for Detection of Inhibitors of Phosphotyrosine Kinases. *Am. Biotech. Lab.* **1998**, *16*, 26–28.
- (40) Hennequin, L. F.; Stokes, E. S. E.; Thomas, A. P.; Johnstone, C.; Ple, P. A.; Ogilvie, D. J.; Dukes, M.; Wedge, S. R.; Kendrew, J.; Curwen, J. O. Novel 4-Anilinoquinazolines with C-7 Basic Side Chains: Design and Structure Activity Relationship of a Series of Potent, Orally Active, VEGF Receptor Tyrosine Kinase Inhibitors. *J. Med. Chem.* **2002**, *45*, 1300–1312.
- (41) Bold, G.; Altmann, K.-H.; Bruggen, J.; Frei, J.; Lang, M.; Manley, P. W.; Traxler, P.; Wietfeld, B.; Buchdunger, E.; Cozens, R.; Ferrari, S.; Furet, P.; Hofmann, F.; Martiny-Baron, G.; Mestan, J.; Rosel, J.; Sills, M.; Stover, D.; Acemoglu, F.; Boss, E.; Emmenegger, R.; Lasser, L.; Masso, E.; Roth, R.; Schlachter, C.; Vetterli, W.; Wyss, D.; Wood, J. M. New Anilinophthalazines as Potent and Orally Well Absorbed Inhibitors of the VEGF Receptor Tyrosine Kinases Useful as Antagonists of Tumor-Driven Angiogenesis. *J. Med. Chem.* **2000**, *43*, 2310–2323.
- (42) Dougher, M.; I. Terman, B. I. Autophosphorylation of KDR in the kinase domain is required for maximal VEGF-stimulated kinase activity and receptor internalization. *Oncogene* **1999**, *18*, 1619–1627.
- (43) *Sybyl 6.9*; Tripos, Inc : St. Louis, MO.
- (44) *OMEGA*; Open Eye Scientific Software: Santa Fe, NM.
- (45) Davidson, N. *Statistical Mechanics*; McGraw-Hill: New York, 1962. McQuarrie, D. A. *Statistical Mechanics*; Harper & Row Inc., New York, 1976.
- (46) Butenandt, A.; Biekert, E.; Haerle, E. Preparation and conversions of 4,5,8-trihydroxy-6-mercaptoquinoline-2-carboxylic acid. *Chem. Ber.* **1964**, *97*, 285–294.

JM050559F